NASA CR-132270

A STUDY OF TRAILING EDGE BLOWING AS A MEANS OF REDUCING NOISE GENERATED BY THE INTERACTION OF FLOW WITH A SURFACE

By Terry D. Scharton
Benjamin Pinkel
John F. Wilby

28 September 1973

BBN Report No. 2593

Prepared under Contract No. NAS1-9559 by

Bolt Beranek and Newman Inc.
21120 Vanowen Street
Canoga Park, California 91303

for

NATIONAL AERONAUTICS AND SPACE ADMINISTRATION

Langley Research Center
Hampton, Virginia

A STUDY OF TRAILING EDGE BLOWING AS A MEANS OF REDUCING NOISE GENERATED BY THE INTERACTION OF FLOW WITH A SURFACE

By Terry D. Scharton
Benjamin Pinkel
John F. Wilby

BBN Report No. 2593

NASA CR-132270

Bolt Beranek and Newman Inc.
21120 Vanowen Street
Canoga Park, California 91303

TABLE OF CONTENTS

LIST OF FIGURES AND TABLES

Figure

Figure

Table

A STUDY OF TRAILING EDGE BLOWING AS A MEANS OF REDUCING NOISE GENERATED BY THE INTERACTION OF FLOW WITH A SURFACE

by Terry D. Scharton
Benjamin Pinkel
John F. Wilby

Bolt Beranek and Newman Inc.

INTRODUCTION

This is the final report on NASA Contract NAS1-9559, Task Order No. 20 (BBN Job No. 11673) and relates to tests on the trailing edge blowing (TEC) concept as a scheme for reducing the noise generated when a jet impinges against a flap.

When a jet stream impinges on a flap at a point upstream of its trailing edge, the series of eddies formed impose alternate zones of positive and negative pressure on the flap surface which move with the flow toward the trailing edge. The sound at frequency f is generated primarily by eddies of length $L = U/f$ where U is the local velocity. For subsonic flow with velocity $U < c$ where c is the speed of sound, the acoustic wavelength $\lambda = c/f$ is longer than the eddy length. The sound field therefore averages over the plus and minus pressure zones and receives little input from the pressure fields on the flap except at the trailing edge where the discontinuity prevents balancing of the alternate positive and negative impulses. In the TEB concept a stream of low-velocity secondary air is ejected from a slot near the trailing edge of the flap as a buffer between the flap and the primary air jet to reduce the intensity of the fluctuating surface pressure field near the flap edge.[1/]

The TEB concept has possible application to the STOL vehicle externally-blown-flap (EBF) configuration. Preliminary tests employing very small primary jet nozzles (diameters 3/16 and 5/8 inches) reported in Ref. 1 indicated that the TEB system reduces the noise generated when a jet impinges on a flap by 6 dB for a primary jet velocity of 500 ft/sec and 4 dB for a primary jet velocity of 900 ft/sec.

The objective of the present program was to determine the effectiveness of the TEB system for a larger scale system with a primary jet nozzle diameter of 8 inches and to obtain some insight into design considerations and noise sources.

Pilot studies on the TEB flap configuration with a 1.25 inch diameter primary jet were made to provide some insight for designing the larger scale (the quarter scale model incorporating a primary nozzle having a diameter of 8 inches) TEB system. Tests of the larger scale TEB system were made to determine its noise abatement effectiveness at primary jet velocities of 700 and 900 ft/sec. Cross-correlation coefficients between the fluctuating pressures on the flap surface and the far-field noise pressures with and without secondary air issuing from the TEB system were determined to locate the primary noise sources on the flap and to provide some insight into the mechanism of noise abatement provided by the TEB system.

The cross-correlation tests to determine the major noise sources were made with a 1/15-scale EBF system comprised of a wing and three flaps not equipped for TEB. The other tests were made on a single flap system configured for the TEB. Tests with 1.25, 1.55, and 1.75-inch diameter primary jets were made at the BBN Canoga Park facility; tests with an 8-inch diameter primary jet were made at the Marquardt facility.

PROGRAMS AND MODELS

Five test programs were conducted.

1) *Simple Turning Flap 1.75-inch Nozzle Diagnostic Tests*

Figure 1 illustrates the simple turning flap used in the first series of tests. This flap has a number of 1/8-inch diameter holes drilled near the flap edge to enable a flush mounted pressure transducer to be inserted from the back of the flap. The holes not in use were sealed with tape during all tests. Provision was also made to measure the fluctuation static pressure in the flap wake using a 1/8-inch microphone with a nose cone. The radiated sound was measured with a 1/2-inch microphone located approximately 1 ft from the nozzle at an angle of 90° from the flap axis. The entire test rig was located in a semireverberant room but the flap, jet, and microphone assembly was surrounded with fiberglass blankets to provide an anechoic condition at the 1/2-inch microphone.

The radiated sound, with and without the flap in place was measured. The surface pressure fluctuations and the pressure fluctuations in the jet exhaust and in the flap wake were determined. Also the real-time cross-correlation between the pressure fluctuations and the radiated sound pressure was measured.

2) *1/15th-Scale Three Flap EBF Model Cross-Correlation Tests*

Cross-correlation coefficients between the far field pressures and the fluctuating pressures on various points on the surface of a 1/15th-scale model of an EBF system (a wing section and three flaps unequipped with a TEB system) were obtained to determine the location of the principle noise sources when the flap system was impacted by an air jet.

The 1/15th-scale wing and flap system model is illustrated in Fig. 2. It was tested in both the takeoff and landing configurations shown in this figure with a 1.55-inch diameter primary nozzle. The nozzle exit velocity used in these tests was 500 ft/sec. Surface pressures were measured with a 0.1-inch diameter BBN piezoelectric transducer which was mounted through holes in the flap (see Fig. 3 for the hole locations) so that the sensitive element was flush with the lower surface of the flap. When not in use, the holes in the flaps were sealed with tape. In the takeoff configuration overlapping of leading and trailing edges of adjacent flaps prevented the taking of data at some locations. The far field sound levels were measured by a B & K 1/2-inch diameter microphone at a distance of 29 inches and an angle of 90° from the jet axis. The readings of the transducer and microphone were recorded in tape and were subsequently cross-correlated. Cross-correlations were also obtained between the readings of two transducers on the flap surface, one held at a fixed position and the other moved to various positions in order to determine the scale of the fluctuating pressure cells.

3) *Small-Scale TEB* Pilot Program*

A pilot program on a small-scale model (1.25-inch diameter nozzle) was conducted to explore briefly the effect of TEB system geometric and flow parameters on the noise abatement provided by TEB. The purpose of this program was to provide data for guiding the design of the larger-scale system (1/4 scale).

A diagram of the flap is shown in Fig. 4. Symbols for the system parameters are defined in Table 1 and are further clarified by Fig. 5.

---

* Trailing-edge-blowing.

The slots at the rear of the upper plate of the flap allowed the wedge at the flap trailing edge to be moved laterally to change dimensions G and M. Shim strips placed between this wedge and the upper plate allowed variation in S. Extension strips attached to the rear of the wedge permitted change in W. Replacement of the wedge by others permitted change in a.

Tests were made at a primary nozzle pressure P_p of 4.5 inch Hg (520 ft/sec) second air pressures P_S from 0 to 12 inch of H_2O, D = 1-1/4 inch, H = 5D, L = D, θ = 45° and values of G from 0.01 inch to 0.10 inch, M from 0.01 inch to 0.25 inch, W from 0.6 inch to 1.0 inch, S from +0.10 to -0.10 inch, and α from 18° to 90°.

4) *Demonstration Test of Larger-Scale TEB (1/4 full scale)*

Tests were made on a model of a flap incorporating TEB system on which impinged a jet frame a jet from an 8-inch diameter nozzle to demonstrate the noise abatement effectiveness of the TEB concept at a scale not far from full-scale and to investigate the effect of several design parameters on noise abatement.

Figure 6 shows the test flap used in this program. Secondary air was provided to a plenum at the leading segment of the flap by a manifold consisting of a 6-inch diameter pipe and five 4-inch diameter tubes. The movable wedge at the trailing edge of the flap permitted adjustments in the slot and flap geometry.

The various flap geometries investigated are shown in Fig. 7. The configuration parameters (see Fig. 5) are:

D = 8 inch
θ = 45°

L = D

H = 5D

S = 0 and 1/4 inch

W = 1.75 and 4.75 inch

In addition an attempt was made to determine for configurations c and g (Fig. 7) whether sharpening the trailing edge as exemplified by configurations h and i, respectively (Fig. 7), would alter the effectiveness of the TEB concept. In configurations h and i, S = 0 and W is 1-3/4 and 4-3/4 inch, respectively. The tests were made with primary jet velocities of 700 and 900 ft/sec and secondary air pressures from 0 to 24 inch H_2O.

5) *Diagnostic Tests of Larger-Scale TEB (1/4 Full Scale)*

Cross-correlation coefficients between the far field pressures and the pressures on the surface of the flap of the 1/4-scale model (Fig. 6) before and after the secondary air slot (Fig. 8) were made with and without secondary air flow to determine whether the reduction in noise provided by TEB could be traced to a drop in the fluctuating pressure at the trailing section of the flap when the secondary air flow is initiated.

The surface pressure sensors were mounted flush with the surfaces on which the primary jet impacts at positions 1 inch upstream and 1 inch downstream of the leading edge of the secondary air slot (see Fig. 8). The secondary air gap G was held at 1/4 inch. The primary jet velocities were 700 and 900 ft/sec. The secondary air pressures varied from 0 to 24 inch of H_2O. The tests were made with the flush and recessed trailing surface configurations illustrated in Figs. 7b and 7c.

FACILITIES

BBN Facility. The small-scale tests (primary jet nozzle diameter between 1 and 2 inches) were made at the BBN Canoga Park test facility. In this facility a diesel-driven reciprocating pump delivers air at a pressure of 100 psi to a plenum chamber located in the test cell, a semireverberant room. The air for the primary and secondary jets was ducted from this plenum to the test model through a sound suppressed valve. Test of the system with the test air mass-flow issuing at low velocity from a large nozzle indicated that the valve noise was indeed negligible compared with the jet noise generated when a test nozzle is used.

Marquardt Facility. Pictures of the Marquardt Facility with the test model in place are shown in Figs. 9 and 10. Air to the model was supplied from a blowdown facility through ducts that were provided with sound suppression liners. Test of the system with the mass flows in the range employed in the tests but with the jet velocities reduced by eliminating the test nozzle at the duct exit indicated that the machinery noise was well below the noise generated by the jet when it issues from the 8-inch test nozzle.

A diagram of the test setup is shown in Fig. 11. The primary nozzle (8-inch diameter) directed the air jet vertically. It was mounted with its exit plane 10 ft from the ground. Two microphones were located each 15 ft from the exit plane of the nozzle, one at the same height as the nozzle and the other at ground level and both in a plane through the nozzle which was normal to the trailing edge of the flap. The flap was at an angle of 45° relative to the exit plane of the nozzle. A polyurethane pad 6 inches

thick, 80 inches long and 150 inches wide was located on the ground under the microphone as shown in Fig. 11 to reduce sound reflections from the ground. This pad was curved over a nearby tank to reduce sound reflections from the tank.

DATA ANALYSIS AND CROSS-CORRELATIONS

Two types of data analysis were employed in this program: 1) 1/3-octave band spectral analysis of the radiated sound and the flap surface pressures, and 2) octave band cross-correlation of the flap surface pressure and the radiated sound and of the flap surface pressures at two positions on the flaps. The instrumentation used is shown in Fig. 12. Since spectral analysis is very common, it is not necessary to describe the details of that process here. However, it is necessary to elaborate on the definition and interpretation of the cross-correlation analysis.

The normalized cross-correlation between pressure signals p_1 and p_2 is defined as

$$C_{p_1 p_2}(\tau) \equiv \frac{\langle p_1(\tau) p_2(t + \tau) \rangle}{[\langle p_1^2(t) \rangle \langle p_2^2(t + \tau) \rangle]^{\frac{1}{2}}} \qquad (1)$$

The signal p_1 is the flap surface pressure and the signal p_2 is alternately the far field sound pressure or the surface pressure at another position. The normalized cross-correlation coefficient ranges between ±1. In the case of surface pressure and far field sound cross-correlations, the peak value of the coefficient occurs at a time delay corresponding to the time it takes for a sound wave to travel the distance R from the surface pressure measurement point to the far field point. In the case of surface pressure cross-correlations, the coefficient peaks at a time delay corresponding to the time

it takes the turbulence to convect the distance ξ from point 1 to point 2. (In the latter case, if the separation ξ is in the spanwise direction, the maximum will occur at a time delay of zero.)

In order to study individually the sources of various frequency components of the radiated sound, it is desirable to filter the jet pressure and far field sound pressure in frequency bands before the cross-correlation indicated by Eq. 1 is performed. The filter bandwidth must be chosen with some care, however, because if the bandwidth is too small the correlation function oscillates and it is difficult to find the maximum value. If both the pressure signals have spectra which are smooth relative to the filter function, the normalized cross-correlation has the form

$$C(\tau) = C_{max} \frac{\sin \pi B(\tau - \tau_m)}{\pi B(\tau - \tau_m)} \cos 2\pi f_o(\tau - \tau_m) \qquad (2)$$

where B is the filter bandwidth in Hz, τ_m is the time delay which the correlation is a maximum, and f_o is the filter center frequency. The cross-correlation function fluctuates at the frequency f_o, the filter center frequency. Therefore the ratio of the value of the correlation at the sidelobes to the maximum value is determined by evaluating Eq. 2 at $\tau - \tau_{max} + 1/f_o$. For octave band filters, which were used exclusively in this investigation, the filter bandwidth B is equal to .707 f_o, and we calculate that octave band filtering results in sidelobes which are approximately 0.36 the value of the maximum.

Cross-correlation of turbulence pressures and far field sound pressures has been previously used as a means of diagnosing the sound radiation properties of pure jets [2] and surfaces in turbulent in turbulent flow [3]. In the case of flap surface pressure and far field sound pressure, the

cross-correlation coefficient normalized as in Eq. 1 has a very simple and useful physical interpretation (see the derivation in the Appendix). The square of the maximum value of the coefficient is the percentage of the mean-square sound radiated to the far field point by the source located at the surface point.

$$C^2_{max} = \% \text{ of } p^2_{rad} \tag{3}$$

A question which is not answered by this surface pressure and far field pressure cross-correlation analysis is "What is the size of the source?" Does the source sit just at the surface pressure measurement point or does it cover the entire surface? The size of the source can be determined however by the cross-correlation of the surface pressures at pairs of points on the surface. The maximum value of the surface pressure correlation coefficient for each separation distance ξ, measured on a straight line, is plotted vs ξ and the source size is defined in terms of the shape of, or the area under this curve.

DISCUSSION OF RESULTS

Simple Turning Flap 1.75-Inch Nozzle Diagnostic Tests

Figure 13 shows the 1/3-octave band spectra of the sound radiated by the jet and flap assembly shown in Fig. 1 and also by the jet alone. The analysis frequencies ranged from 200 Hz < f < 31,500 Hz.

Figure 14 shows 1/3-octave band spectra of the pressure measured at two positions near the flap edge, at two positions in the wake of the flap, and in the jet with the flap removed. The surface pressure spectra measured 1-1/2 inch and 1/4 inch upstream of the flap edge are almost identical over the entire

frequency range. The pressure spectra measured 3/4 inch and 1-1/2 inch downstream of the flap in the wake show somewhat higher pressure levels than those measured on the flap surface. This sudden increase in the pressure levels as one moves downstream of the edge might be closely associated with the noise generation process. Perhaps the most interesting result presented in Fig. 14 is that the pressure spectrum measured 5 nozzle diameters downstream on the centerline of the free jet is very similar to the spectra measured on the flap surface over a broad frequency range. This result is particularly astounding in view of the large difference in the sound radiated by the free jet and the jet plus flap as shown in Fig. 13. This similarity also lends credence to the view that the noise is generated by the interaction of the *free jet* turbulence with the flap edge rather than by the interaction of the flap turbulent boundary layer with the edge or rather than by flap wake turbulence effects.

Figure 15 shows direct cross-correlations between the surface pressures measured at various positions relative to the edge of the simple flap shown in Fig. 1 and the radiated sound. The surface pressure p_o and the radiated pressure p were first filtered in octave bands and then processed with a Honeywell correlator which delays the surface pressure signal at time τ, multiplies the two signals, and averages the product. The maximum cross-correlations shown in Fig. 15 were obtained at a time delay τ_{max} corresponding to the time it took an acoustic wave to propagate from the surface transducer to the microphone. The cross-correlations plotted in Fig. 15 were normalized according to

$$C_{p_o p}(\tau)_{max} \equiv \frac{\langle p_o(t)p(t+\tau)\rangle_t}{[\langle p_o^2(t)\rangle_t \langle p^2(t+\tau)\rangle_t]^{\frac{1}{2}}}$$

As indicated in the Appendix, the square of the normalized cross-correlation coefficient as defined above may be interpreted as the "fraction of the mean square sound received at the far field microphone which was generated at the surface pressure sensor location." Alternatively the reciprocal of the squared coefficient may be viewed as approximately the "number of independent sources contributing to the measured radiated sound." The latter interpretation of the cross-correlation coefficient is approximate because the interpretation is based on the assumption that the surface pressure field is homogeneous, that is, that all the sources are the same size and strength. The data in Fig. 15 predicts approximately 4 independent sources at 2000 Hz, 6 at 4000 Hz, 20 at 8000 Hz, and 50 at 16,000 Hz.

The data presented in Fig. 15 constitutes direct evidence that the sound is generated near the edge of the flap, with the high frequency sources located nearer the edge than the low frequency sources. If for convenience we adopt the view that the sources are lined up one deep, spanwise along the edge essentially filling the high velocity region of the jet, we can infer the source size as a function of frequency from this data. If we assume that the jet is approximately 2 nozzle diameters or 3.5 inches wide at the edge then we compute source sizes of 0.9 inches at 2000 Hz, 0.6 inches at 4000 Hz, 0.17 inches at 8000 Hz, and 0.07 inches at 16,000 Hz.

These calculations lead us to postulate an approximate empirical relation between the source size and frequency given by

$$L \simeq 0.5\ U/f$$

where L is the source size, U is the local velocity, and f is frequency. Assuming a local average velocity of approximately 80% of the nozzle exit velocity this relation predicts

source sizes of approximately 1 inch at 2000 Hz, 0.5 inch at 4000 Hz, 0.25 inch at 8000 Hz, and 0.125 inch at 16,000 Hz. The source sizes predicted from this relation are also shown as ticks at various distances back from the trailing edge in Fig. 15. Note that the postulated relation implies that the source size important at a given frequency depends only on velocity, not on nozzle size! The nozzle size only determines the distribution of energy among source sizes or alternately among frequencies.

1/15th-Scale Three Flap EBF Model Cross-Correlation Tests

The 1/15th-scale model shown in Fig. 2 was used in these tests. The location of the pressure sensor holes are shown in Fig. 3. The tests were made with a 1.55 inch diameter convergent nozzle from which air was discharged at a velocity of 500 ft/sec. Both the landing and takeoff configurations shown in Fig. 2 were investigated.

Far field sound levels were measured using a B & K 1/2-inch diameter microphone at a distance of 29 inches, and an angle of 90°, from the jet axis. Surface pressures were measured with a BBN 0.1-inch diameter piezoelectric transducer which was mounted through holes in the flaps so that the sensitive element was flush with the lower surface of the flap. When not in use, the holes in the flaps were sealed with tape. In the takeoff configuration, overlapping of leading and trailing edges of adjacent flaps prevent the taking of data at some locations. Transducer positions used for the surface pressure measurements are indicated in Fig. 3.

Far field sound levels in one-third octave bands, are compared in Fig. 16 for the jet alone and for the EBF in takeoff and landing configurations. The one-third octave

band center frequencies are shown in terms of the nondimensional Strouhal number. One-third octave band levels for the jet alone are at least 8 dB below the sound levels for the EBF; for frequencies in the range 200 Hz to 10,000 Hz the difference is at least 10 dB. Thus interference from upstream noise in the jet air supply should be negligible.

Maximum correlations between the surface pressure fluctuations and the far field are contained in Figs. 17 and 18 for the three flaps and two configurations. Data for the takeoff configuration are not complete because of the overlapping of the flaps. Figure 18 identifies the leading edge of the third flap as the major contributor to the far field noise on approach, with the leading and trailing edges of the second flap being next in importance. In the takeoff configuration, the trailing edge of the third flap becomes a much more important contributor to the far field sound levels; unfortunately it was not possible to measure the corresponding contribution of the leading edge.

Spatial cross-correlations of the pressure field on the trailing edge of the third flap are shown in Fig. 19 for the two flap configurations. The correlations were performed in octave band widths with center frequencies in the range 1000 Hz to 16,000 Hz, and were normalized with respect to the octave based rms pressures at each transducer location. Location 3C1 on the flap (see Fig. 3) was taken as the datum location for the separation distance. To estimate the area under each curve, and hence the spanwise integral scale lengths for the pressure field, inverse exponential functions were fitted to the experimental data as shown in Fig. 19. The resulting integral scale lengths are shown in Table II. If a relationship of the form $\Lambda \alpha f^{-\beta}$ is assumed, then β lies in the range 0.6 to 1.6 and increases with frequency.

Figure 20 shows the correlation of the surface pressure on the trailing and leading edge of adjacent flaps. These data indicate the degree to which the leading edge noise source of a downstream flap might be controlled by blowing the trailing edge of the adjacent upstream flap.

Small-Scale TEB* Pilot Program

These pilot tests were conducted with a 1.25-inch diameter nozzle using the flap shown in Figs. 4 and 5. Figure 21 is representative of the best performance obtained in these pilot tests. This figure shows noise reductions of from 3 to 6 dB, the greater reductions occurring at the higher frequencies.

Noise reduction data obtained with other configurations (see list of parameter ranges on page 5) supported the following conclusions:

1) Decreasing the distance W from the slit to the trailing edge raised the frequencies at which blowing was effective.

2) If the primary air pressure is increased, the secondary air pressure must be increased proportionally for comparable performance.

3) The width of the slot B need be only approximately one or two nozzle diameters wide for high frequency noise reduction.

4) The most sensitive (and least understood) parameter which affects the noise reduction potential of TEB appears to be the angle α of the secondary air relative to the surface. Tests with smaller angles

than 18°, nearly parallel flow, resulted in degraded performance as did tests with very large angles near 90°, perpendicular flow.

In the small-scale tests using the flap model shown in Fig. 4, the presence of the slot, with no secondary air flow, resulted in an increase in the noise over that for an unslotted flap. Therefore the baseline case in Fig. 21 is taken to be an unslotted flap.

Demonstration Test of Larger-Scale TEB (1/4 Full Scale)

Using the flap model shown in Fig. 6, the 10 TEB configurations shown in Fig. 7 were tested at the Marquardt Company facility shown in Figs. 9, 10, and 11 at primary jet exit velocities of 700 and 900 ft/sec.

Figure 22 shows the noise reduction obtained with the most effective configuration tested (the configuration shown in Fig. 7b) compared with the noise generated by a flap with the slot sealed (configuration 7a). In contrast to the results obtained in the small-scale tests, the 1/4-scale test data indicated that the presence of the slot with zero flow resulted in slightly less noise than did the flap with the slot sealed. Secondary blowing resulted in approximately 2 dB reduction in the overall noise and 3 to 6 dB noise reduction in the high frequencies. The maximum potential of the TEB technique was probably not realized in the high frequency range, because there the flap noise is reduced to that of the jet alone.

The overall noise reduction of the other 8 configurations tested is given in Fig. 7. Most of those configurations resulted in considerably less noise reduction in the high frequency range than did the configuration associated with

the data of Fig. 22. Data obtained with the higher exit velocity of 900 ft/sec indicated generally less noise reduction and the largest noise reductions achieved with the higher exit velocity came with the use of the largest secondary pressure.

Diagnostic Tests of Larger-Scale TEB (1/4 Full Scale)

The surface pressure 1 inch upstream and 1 inch downstream of the 1/4-scale configuration 7 B flap was measured with the 0.10 inch BBN pressure transducers as shown in Fig. 8, and the results are shown in Fig. 23. Secondary blowing reduced the surface pressures by 6-12 dB over generally the complete analysis frequency range, both upstream and downstream of the slot. It is puzzling that secondary blowing has twice as much effect on the surface pressures as on the radiated sound. This relatively large effect of blowing on the surface pressure supports the intuitive feeling that TEB provides a relatively convenient handle for affecting the noise sources. However, the smaller effects of TEB on the radiated noise suggests that we have not yet discovered the optimum position of the crank.

The surface pressures upstream and downstream of the slot on the 1/4-scale model were cross-correlated with the radiated sound pressure to determine the relative importance of the sources located upstream and downstream of the slot and the effect of blowing on these sources; the results are shown in Table III.

The data in Table III for both configurations 7 B and C indicate that the region downstream of the slot is the most important noise generator (overall and in the 1000 Hz band) both with and without TEB. Secondary blowing had a significant effect in reducing the contribution of the upstream

sources but little effect on the downstream sources. This result suggests more investigation of the configuration shown in Fig. 7i, in which the slot is located at the trailing edge.

REFERENCES

1. B. Pinkel and T. D. Scharton, "Reduction of Noise Generated by Flow of Fluid Over Plate," presented at the 84th Meeting of the Acoustical Society of America, Miami Beach, Florida, November 29, 1972.

2. T. D. Scharton and P. H. White, "Simple Pressure Source Model of Jet Noise," submitted to the *Journal of the Acoustical Society of America,* February 1972.

3. Thomas E. Siddon, "Surface Dipole Strength by Cross-Correlation Method," *J. Acoust. Soc. Am.* 53, 2, p. 619, February 1973.

TABLE I

NOMENCLATURE

D	inside diameter of primary nozzle, inch
H	distance from nozzle exit to flap along nozzle axis, inch
L	distance from intersection of nozzle axis with flap and forward edge of slot, inch
G	slot gap width measured across narrowest section, inch
M	width of slot in direction of plate surface, inch
W	distance from rear of slot to trailing edge, inch
B	width of slot, inch
S	height of face of trailing section of flap relative to main face of flap, inch
θ	angle of flap relative to nozzle axis
α	angle of ramp forming rear face of slot
P_p	primary total pressure into nozzle in Hg
P_s	secondary total pressure into slot in H_2O

TABLE II

INTEGRAL SCALE LENGTHS FOR PRESSURES ON TRAILING EDGE OF FLAP #3

Frequency (Hz)	Scale Length Λ (inch) Takeoff Config.	Landing Config.
1000	1.21	0.61
2000	0.88	0.46
4000	0.51	0.30
8000	0.25	0.16
16,000	0.09	0.05

TABLE III

CROSSCORRELATION TESTS (MARQUARDT INSTALLATION)

Primary Total Pressure 4.5 psi

Configuration B (see Fig. 7)

Pressure sensor location	Secondary pressure inch H_2O	C		% P^2	
		Overall	1000 Hz	Overall	1000 Hz
I	0	.258	.116	0.067	0.013
I	3	.202	.092	0.041	0.0085
I	24	.179	.061	0.032	0.0037
II	0	.43	.27	0.185	0.073
II	3	.54	.29	0.292	0.084
II	24	.65	.25	0.423	0.063

TABLE III (Continued)

Configuration C (see Fig. 7)

Pressure sensor location	Secondary pressure inch H_2O	C		$\%P^2$**	
		Overall	1000 Hz*	Overall	1000 Hz*
I	0	0.61	0.45	0.372	0.203
I	3	.41	.19	0.168	0.036
I	6	.43	.21	0.185	0.044
I	24	.49	.19	0.240	0.036
II	0	.65	.37	0.423	0.137
II	3	.65	.31	0.423	0.096
II	24	.67	.31	0.449	0.096

* Octave centered at 1000 Hz.

** $\%P^2 = C^2$ is percentage of noise P^2 attributable to fluctuating pressures near pressure sensor points.

I Pressure sensor 1 inch upstream of secondary air slot.

II Pressure sensor 1 inch downstream of secondary air slot.

APPENDIX

INTERPRETATION OF NORMALIZED CROSSCORRELATION BETWEEN SURFACE TURBULENCE PRESSURE AND FARFIELD ACOUSTIC PRESSURE

The acoustic pressure $p(R,\theta;t)$ radiated to a farfield point at distance R and angle θ from a rigid surface exposed to a turbulence pressure field $p_o(\bar{S},t)$ is

$$p(R,\theta;t) = \frac{-\cos\theta}{4\pi c_o R} \int_{\bar{S}} \frac{\alpha}{\alpha t} p_o\left(\bar{S};t - \frac{R}{c_o}\right) d\bar{S} \qquad \text{(A-1)}$$

for the case where the characteristic dimensions of the wetted surface are small compared to the distance to the farfield observation point.[A-1]

For fixed $\bar{R}$ and filter frequency ω, we may write:

$$p(\bar{R},\omega) = \sum_{i=1}^{N} p_o^i(\bar{R},\omega) s^i(\omega) \qquad \text{(A-2)}$$

The farfield pressure is the sum of the contributions from N independent surface pressures p_o^i, with s^i given by Eq. (A-1) as:

$$s^i \equiv \frac{\sqrt{-1}\ \omega \cos\theta\ S^i}{4\pi c_o R} \qquad \text{(A-3)}$$

The surface area S^i appropriate to the ith surface pressure contribution is defined by:

$$\langle p_o^i p_o^j \rangle = \delta_{ij} (p_o^i)^2 \qquad \text{(A-4)}$$

where δ_{ij} is the Kroneker-Delta function.

The mean-square farfield filtered acoustic pressure is

$$\langle p^2 \rangle = \sum_{i=1}^{N} \langle p_o^i p \rangle s^i \quad , \tag{A-5}$$

so that the ith surface element makes a contribution $\langle p^2 \rangle^i = \langle p_o^i p \rangle s^i$. The *percentage* of the mean-square acoustic pressure at $\bar{R}$ contributed by the ith element is then:

$$\% = \frac{\langle p_o^i p \rangle s^i}{\langle p^2 \rangle} \quad , \quad \text{or} \tag{A-6}$$

$$\% = \frac{\langle p_o^i p \rangle^2}{\frac{1}{s^i} \sum_{j=1}^{N} \langle p_o^i p_o^j \rangle s^j \quad \langle p^2 \rangle} \quad , \quad \text{or}$$

$$\% = \frac{\langle p_o^i p \rangle^2}{\langle p_o^{i2} \rangle \langle p^2 \rangle} = C^2_{p_o p}(\tau^*) \tag{A-7}$$

where τ^* would be the retardation time $\tau = \frac{R}{c}$ in the absence of convection effects. With convection the appropriate time delay τ^* at which $c_{p_o p}$ is maximum varies slightly from R/c. This concludes the proof of Eq. (3) in the text.

If one further assumes that all N sources contribute equally to the sound radiated to R, i.e., $\langle p_o^i \rangle^2 s^i$ is independent of i, then the number of independent sources is the reciprocal of the percentage each contributes:

$$N = 1/\% = 1/C^2_{p_o p}(\tau^*) \tag{A-8}$$

Appendix Reference

A-1. Thomas E. Siddon, "Surface Dipole Strength by Cross-Correlation Method," *J. Acoust. Soc. Am.* 53, 2, p. 620, Eq. 4, February 1973.

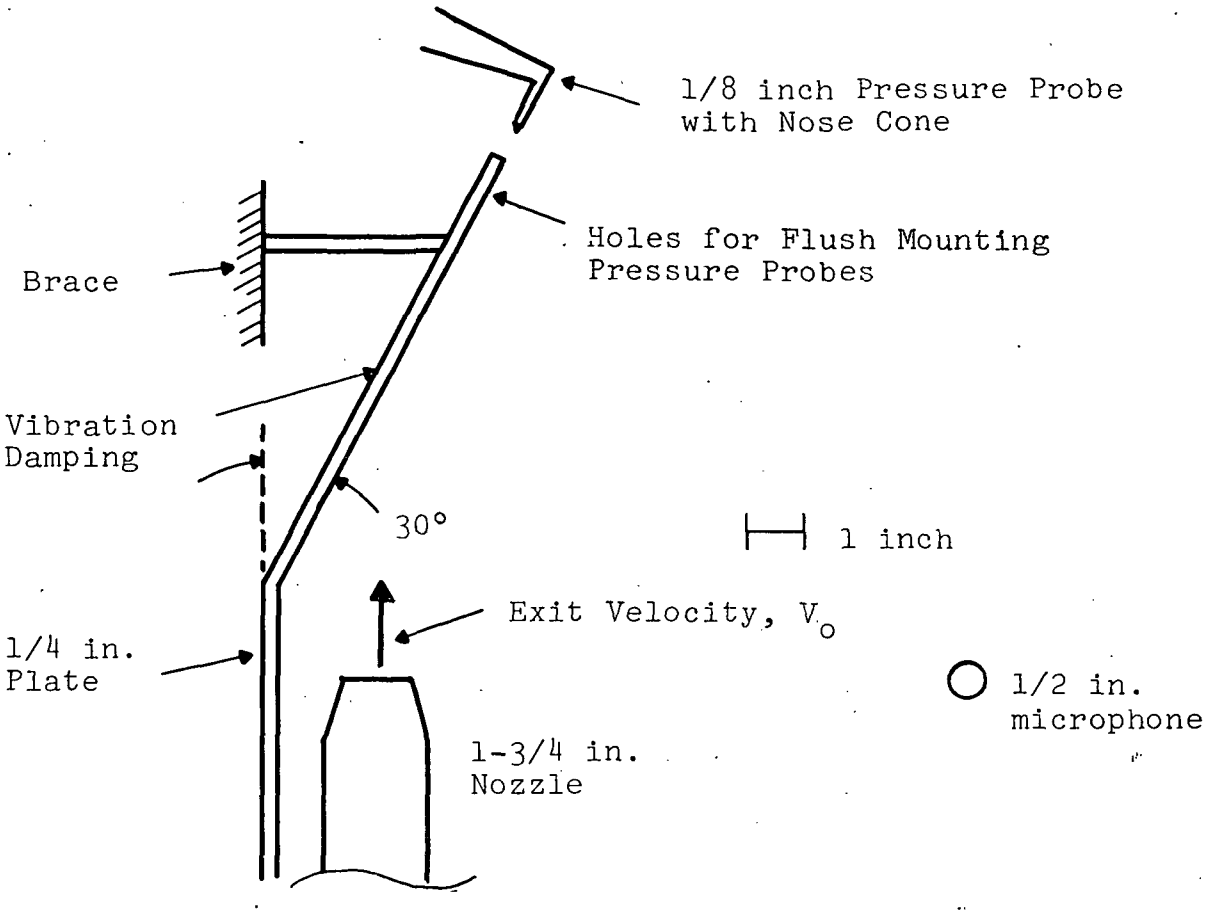

FIGURE 1a. Side View of Jet and Plate Test Setup

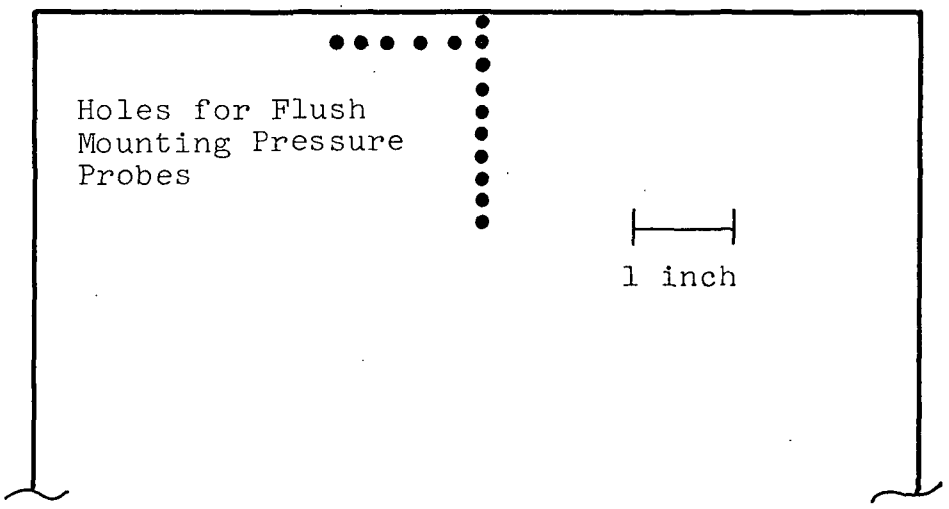

FIGURE 1b. Front View of Top Portion of Plate

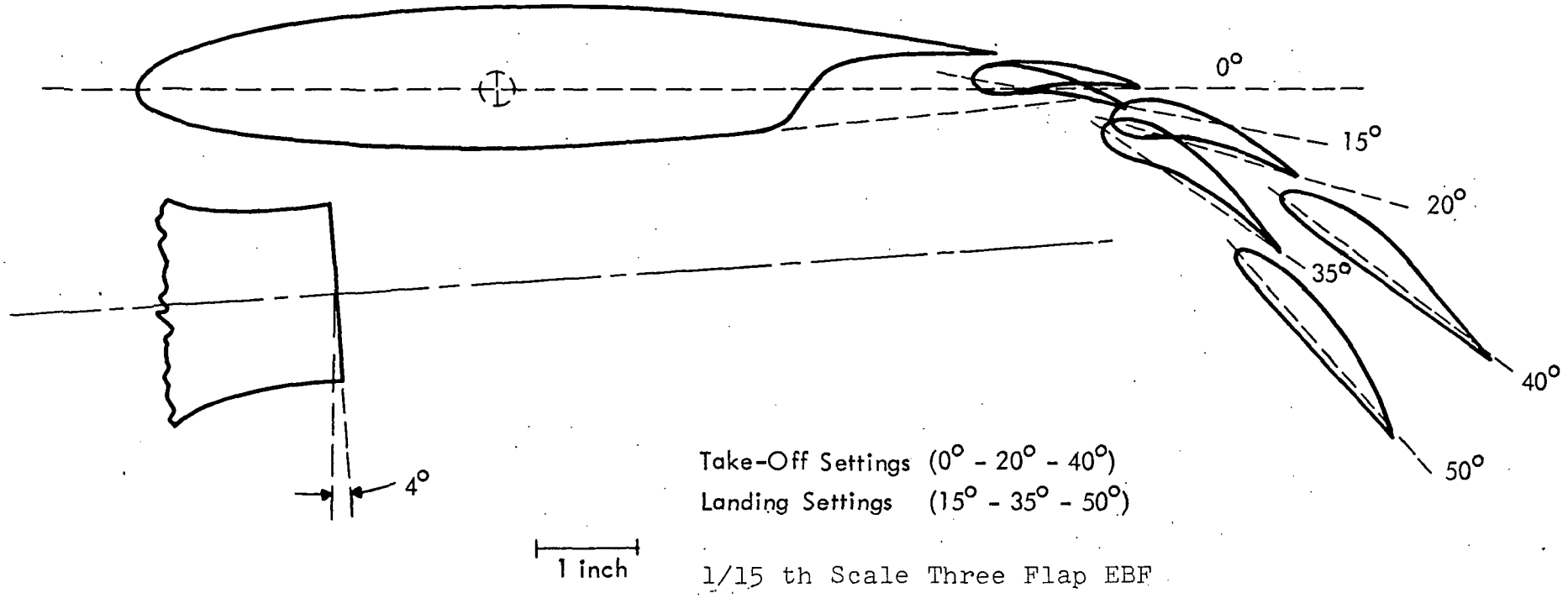

FIGURE 2. EXPERIMENTAL CONFIGURATION

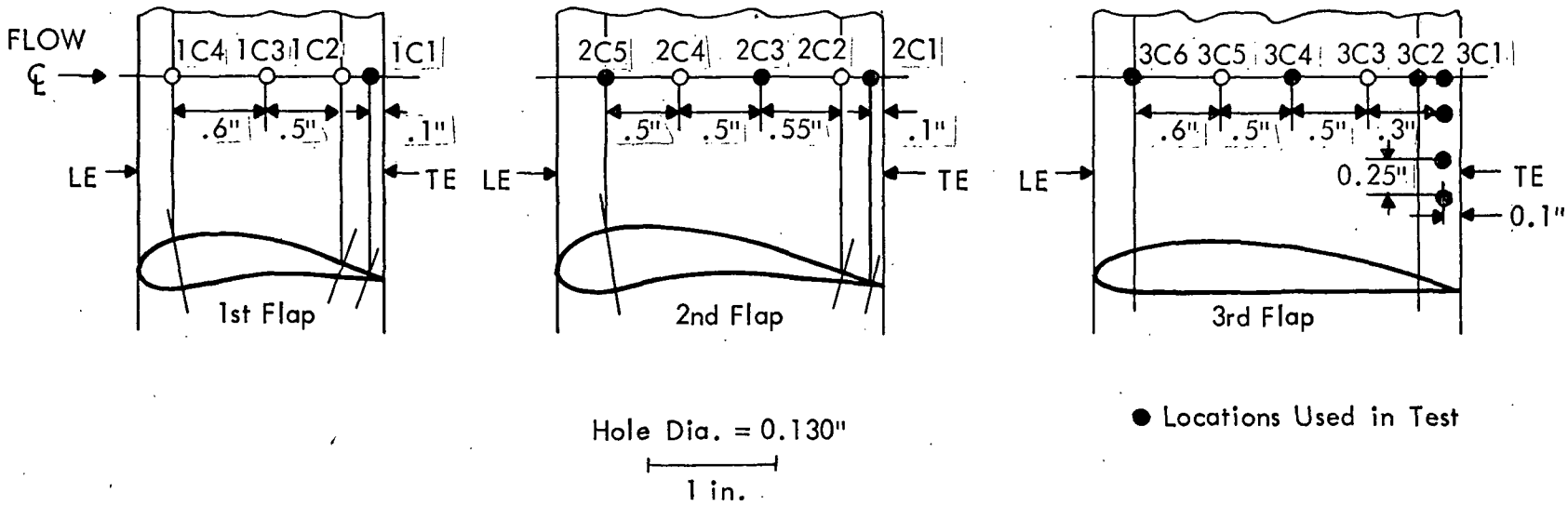

FIGURE 3. SCHEMATIC OF SURFACE PRESSURE SENSOR LOCATIONS AND DESIGNATIONS (1/15 Scale EBF)

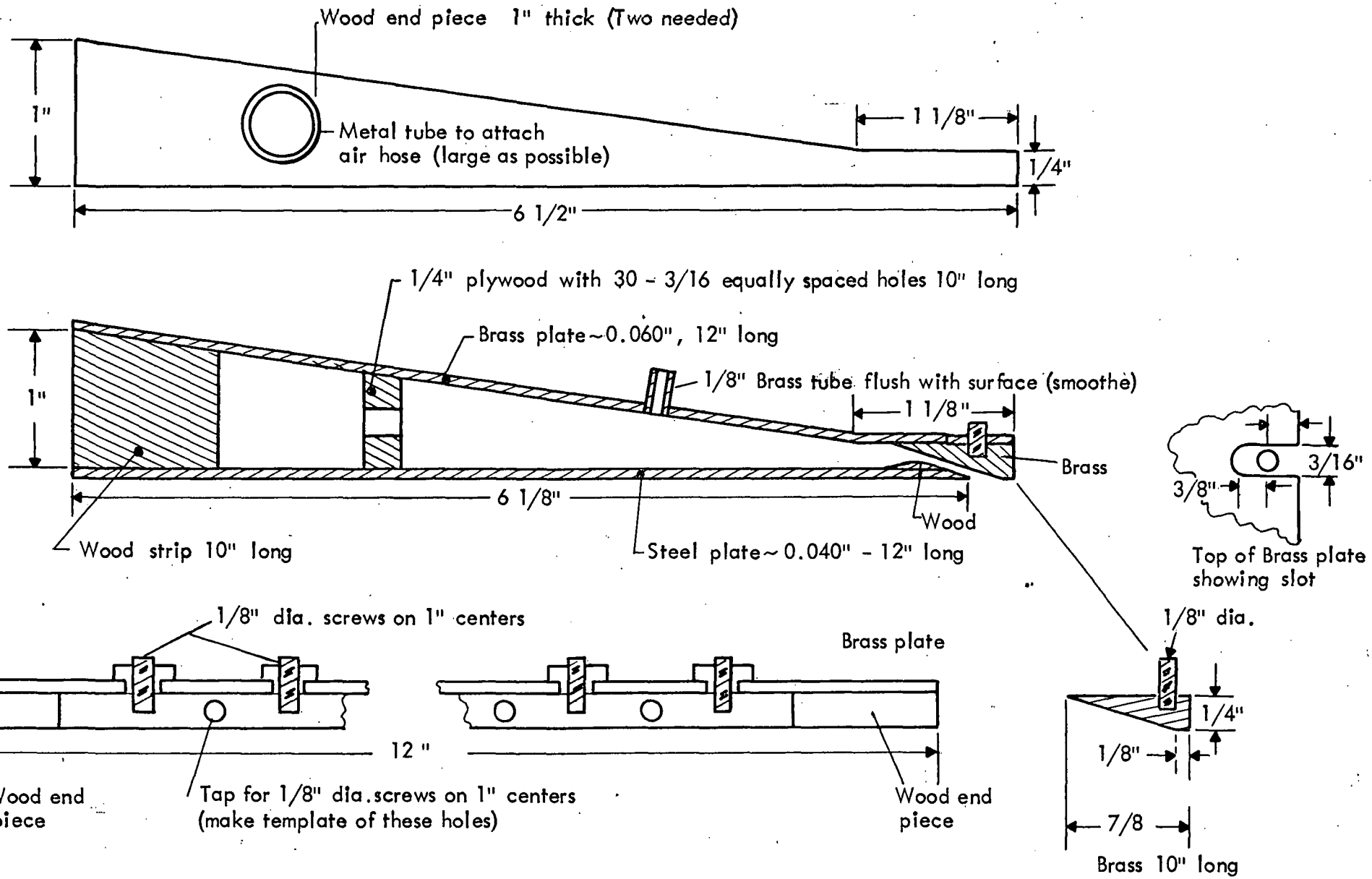

FIGURE 4. SLOTTED FLAP TEST MODEL FOR 1.25" NOZZLE

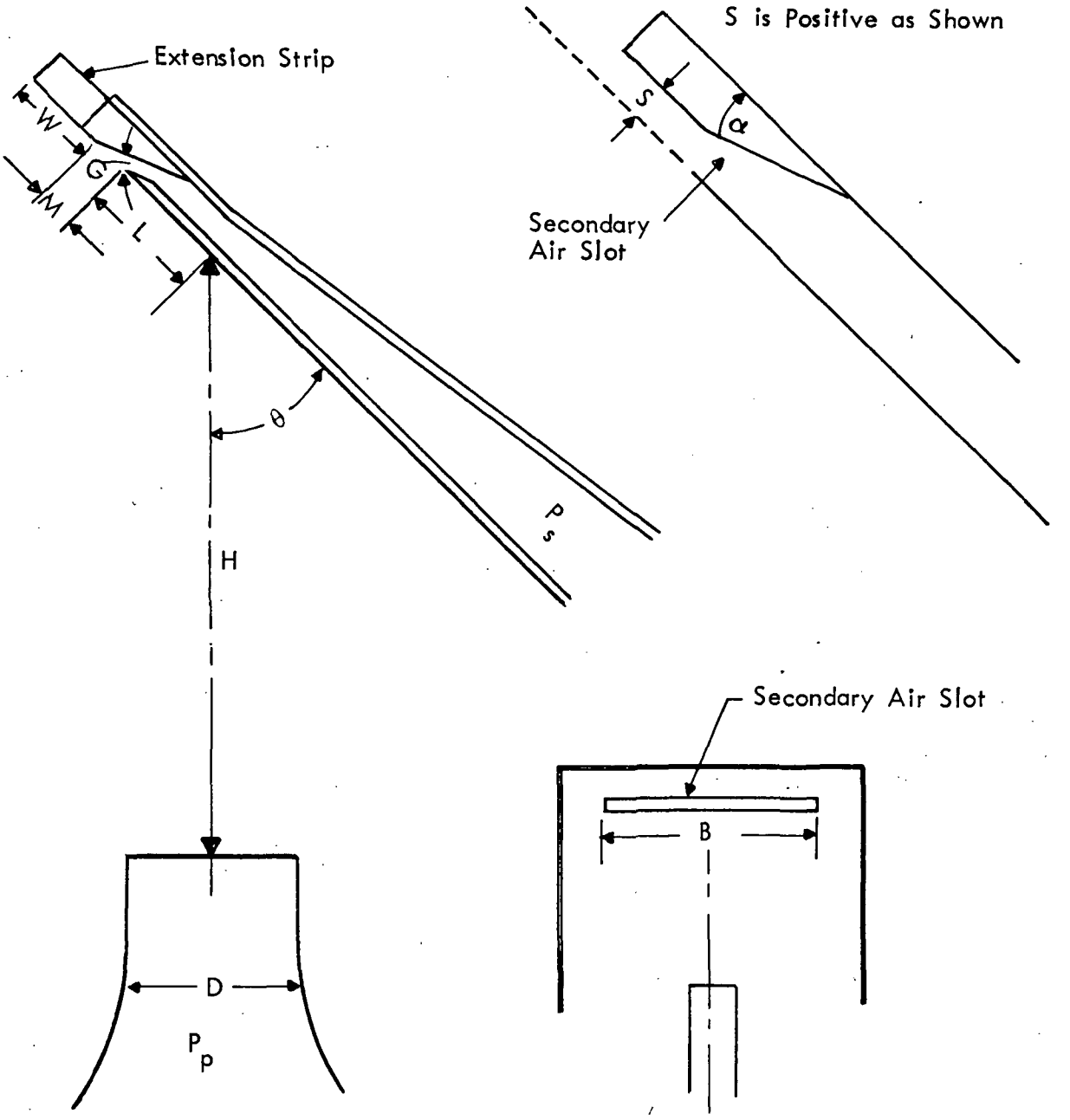

FIGURE 5. PARAMETERS IN SLOTTED FLAP TESTS

a) SIDE VIEW

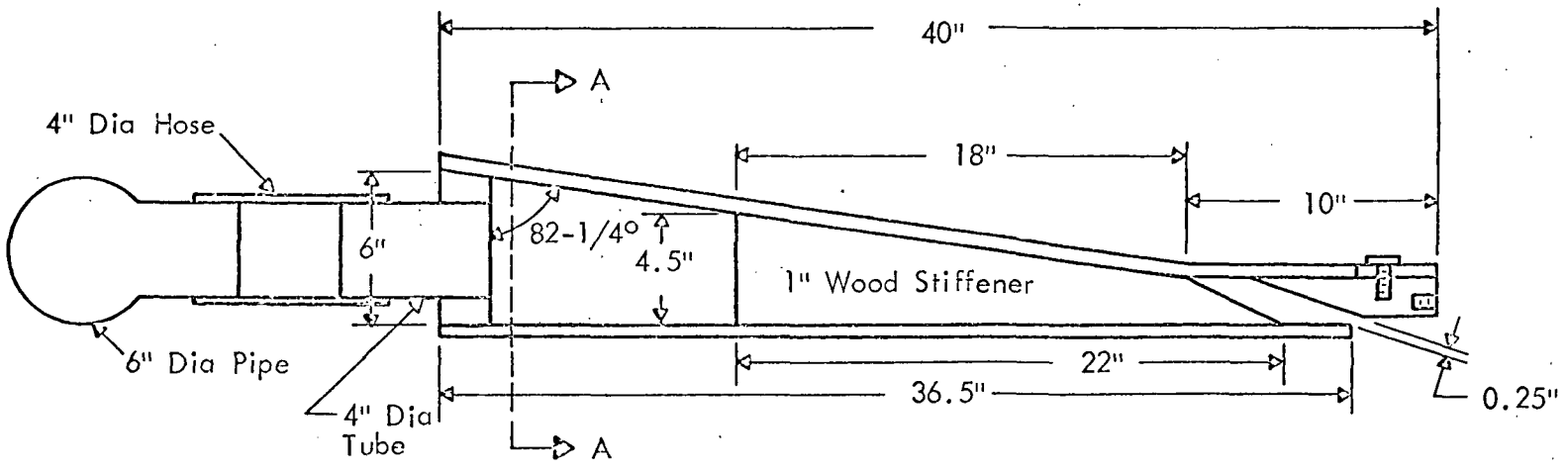

b) END VIEW

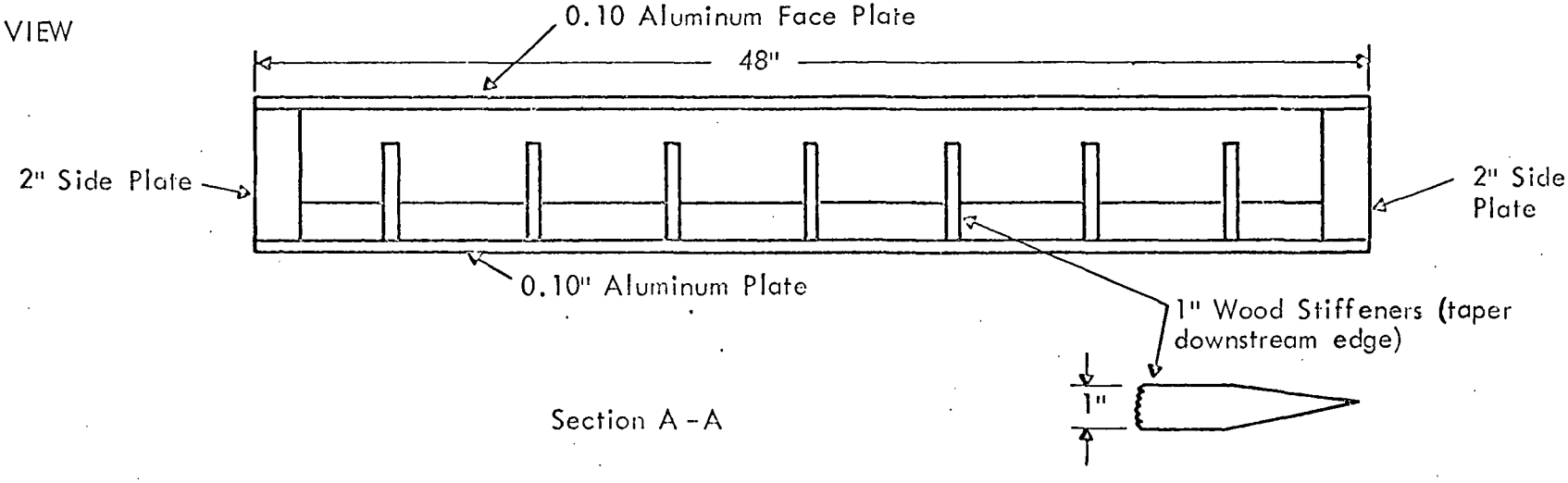

FIGURE 6. TEST MODEL FOR 8" NOZZLE DIAMETER MARQUARDT FACILITY

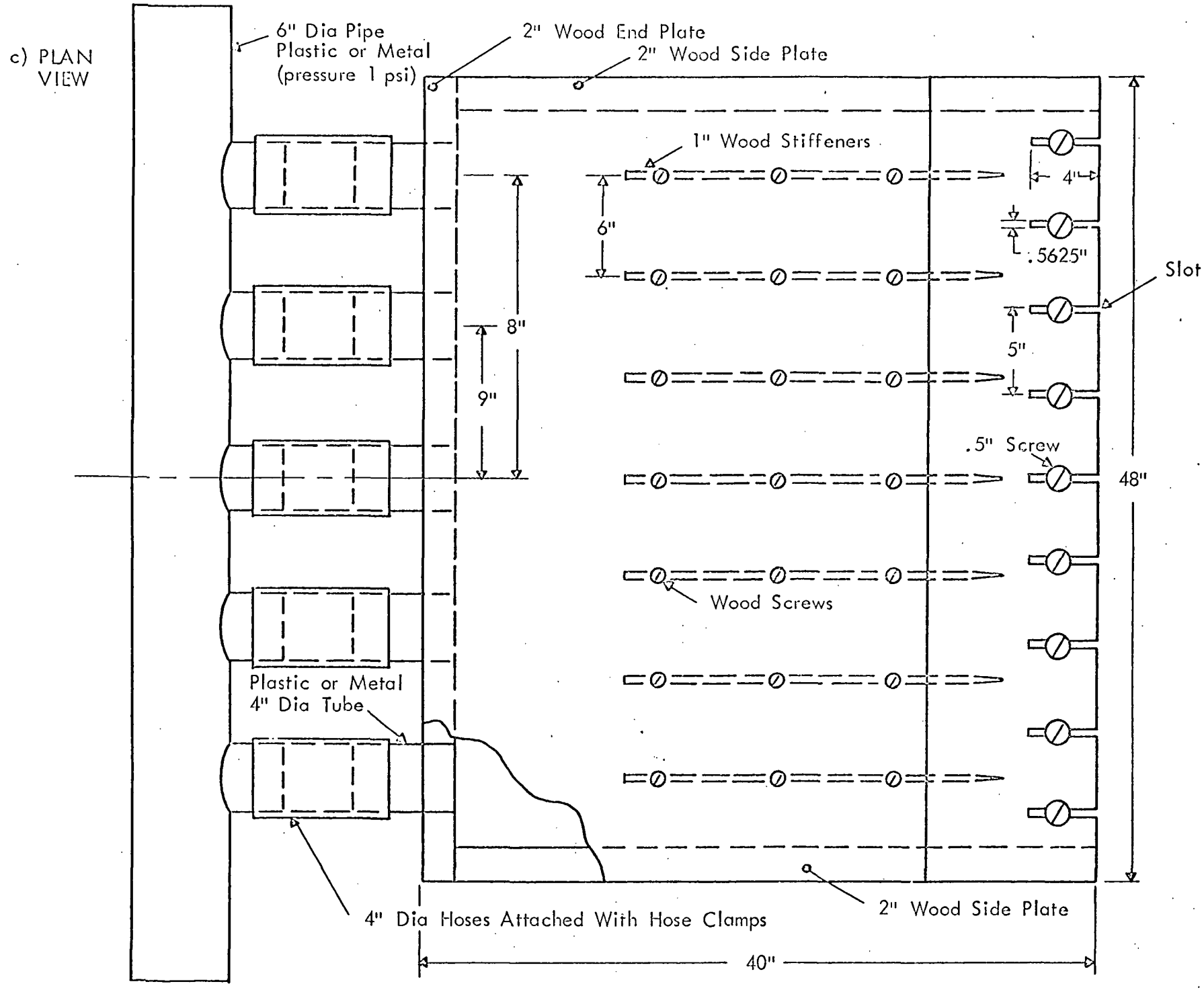

FIGURE 6. (Continued)

d) WEDGE INSERT AT TRAILING EDGE

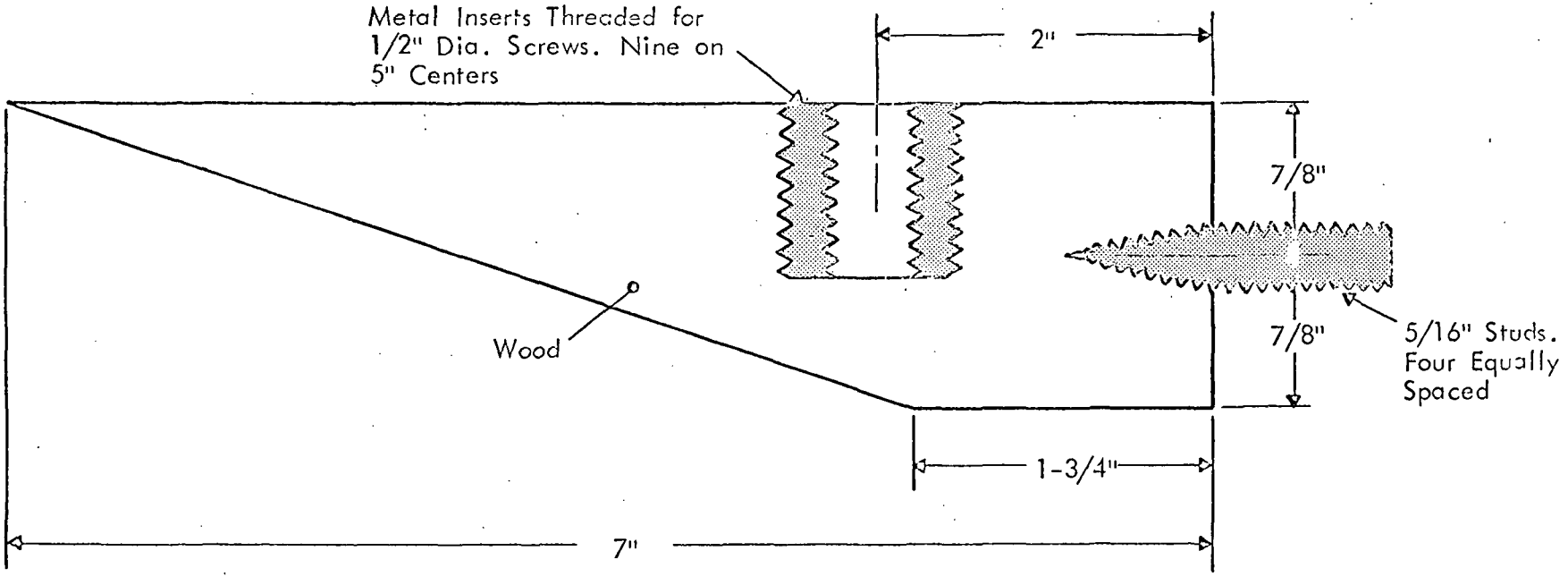

Glue or cement or use other method of fastening metal insert onto wood, 9 holes on 5" center at each location.

FIGURE 6. (Continued)

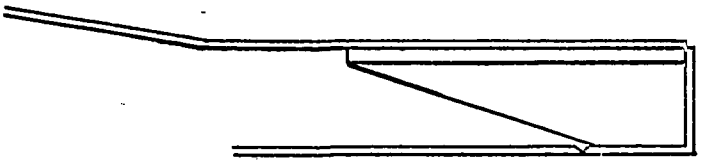

a) Secondary Slot Sealed Shut Reference Condition

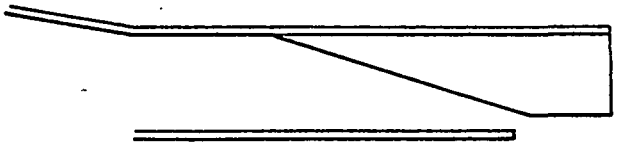

b) Basic Wedge
(Recessed Trailing Surface)
(2 dB OV)

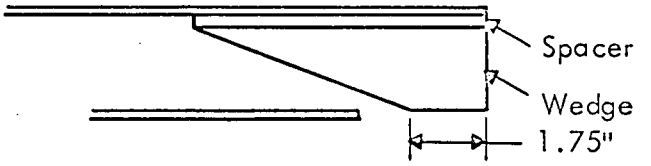

c) Basic Wedge with Spacer
(Flush Trailing Surface)
(1 dB OV)

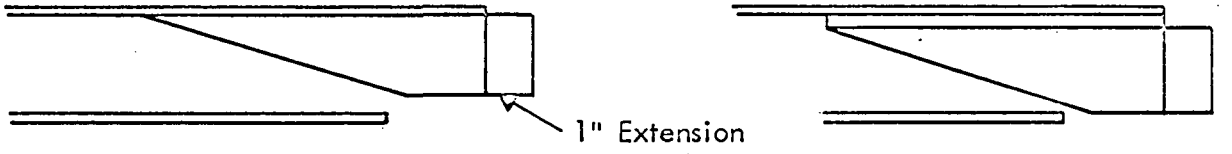

d) Wedge Plus 1" Extension
(2 dB OV)

e) Wedge Plus 1" Extension Plus
Spacer (1 dB OV)

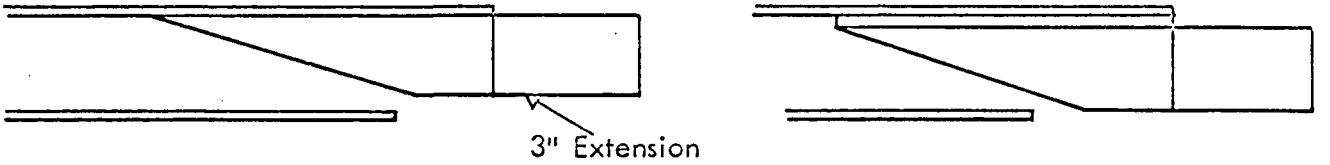

f) Wedge Plus 3" Extension
(1 dB OV)

g) Wedge Plus 3" Extension Plus
Spacer (2 dB OV)

FIGURE 7. TRAILING EDGE TEST CONFIGURATIONS

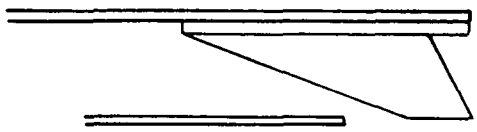

(h) BASIC WEDGE WITH SHARPEND TRAILING EDGE PLUS SPACER

(1 dB OV)

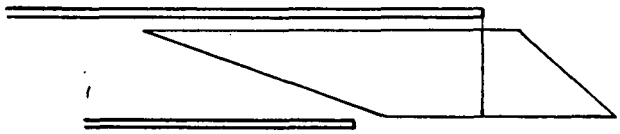

(i) WEDGE PLUS 3" EXTENSION WITH SHARPEND TRAILING EDGE PLUS SPACER

(1 dB OV)

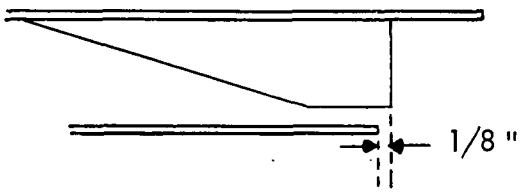

(j) SAME AS CONFIGURATION b WITH WEDGE SLID FORWARD

(1 - 2 dB OV)

FIGURE 7. CONTINUED

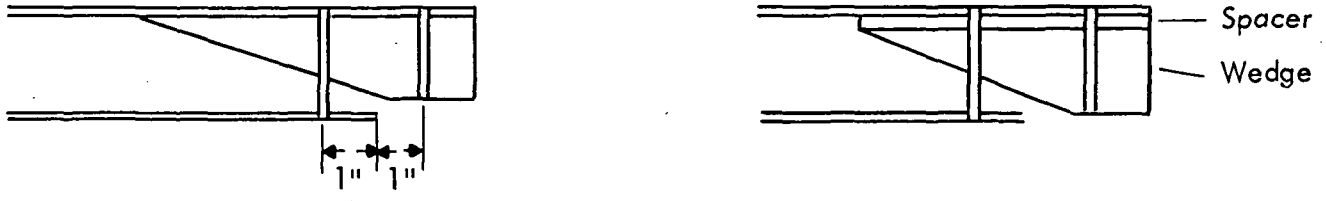

FIGURE 8. LOCATION OF FLUCTUATING PRESSURE SENSORS ON FLAP BEFORE AND AFTER SLOT FOR SURFACE PRESSURE MEASUREMENTS

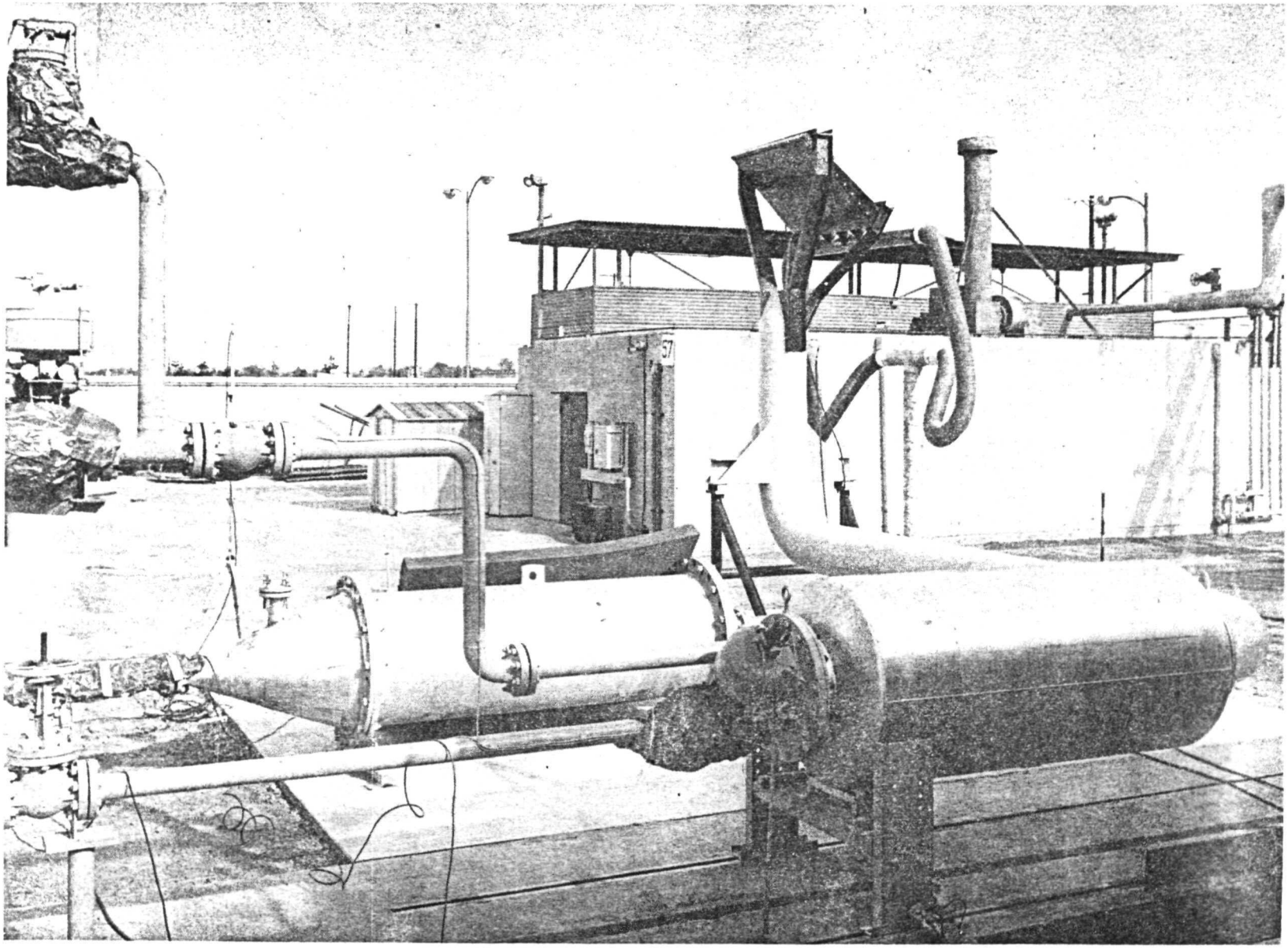

FIGURE 9. MARQUARDT TEST RIG (SIDE VIEW)

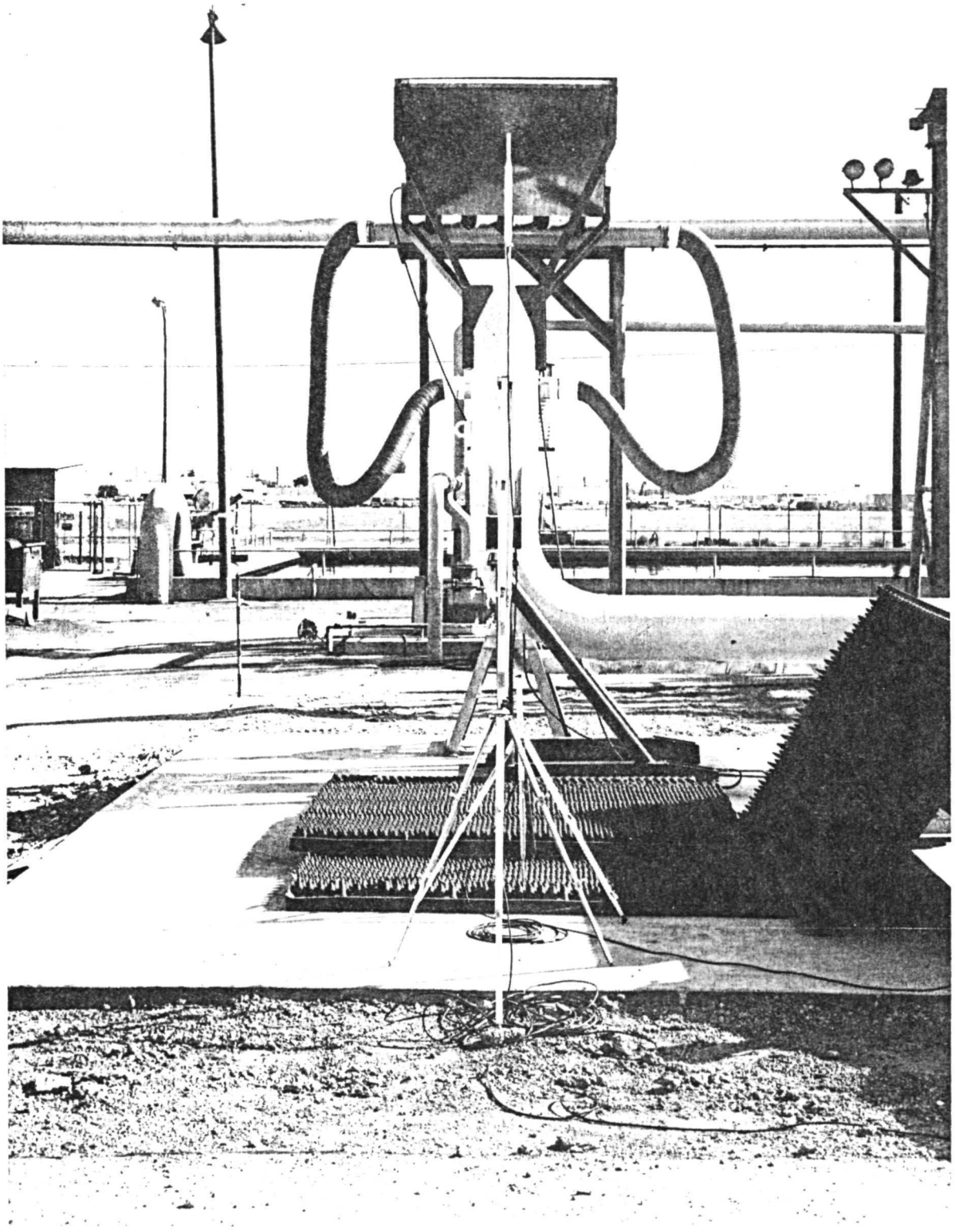

FIGURE 10. MARQUARDT TEST RIG (FRONT VIEW)

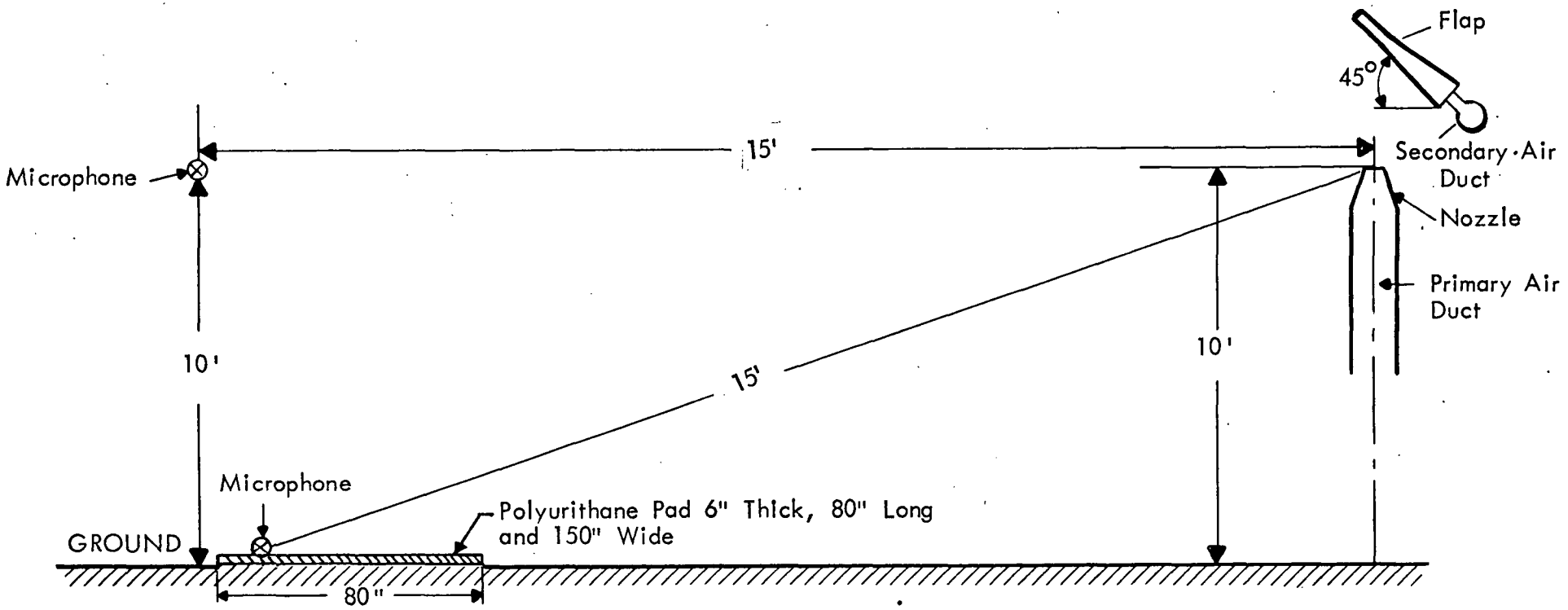

FIGURE 11. DIAGRAM SHOWING LOCATION OF MICROPHONES IN SET-UP IN MARQUARDT TEST FACILITY

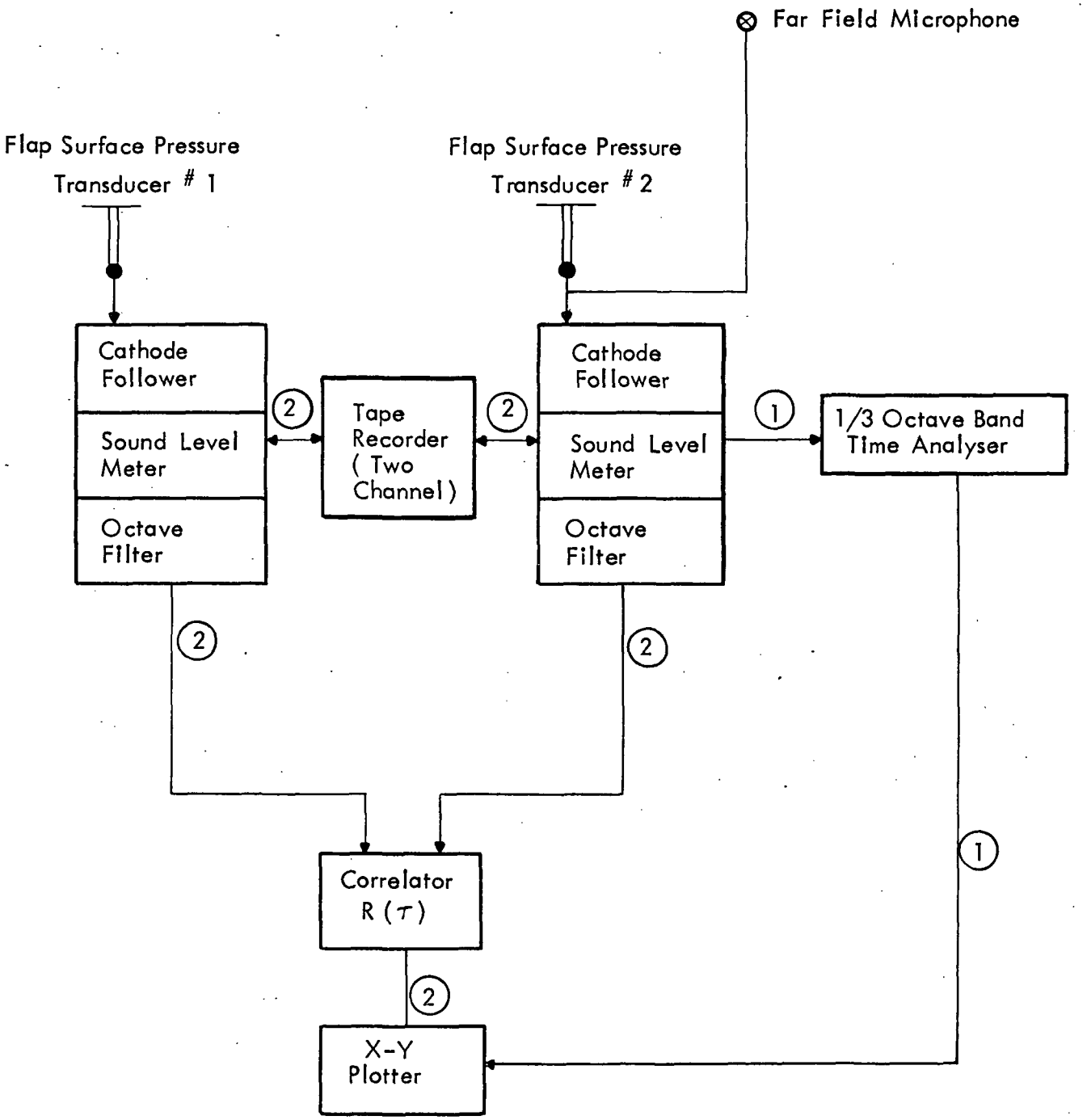

FIGURE 12. DATA ANALYSIS EQUIPMENT

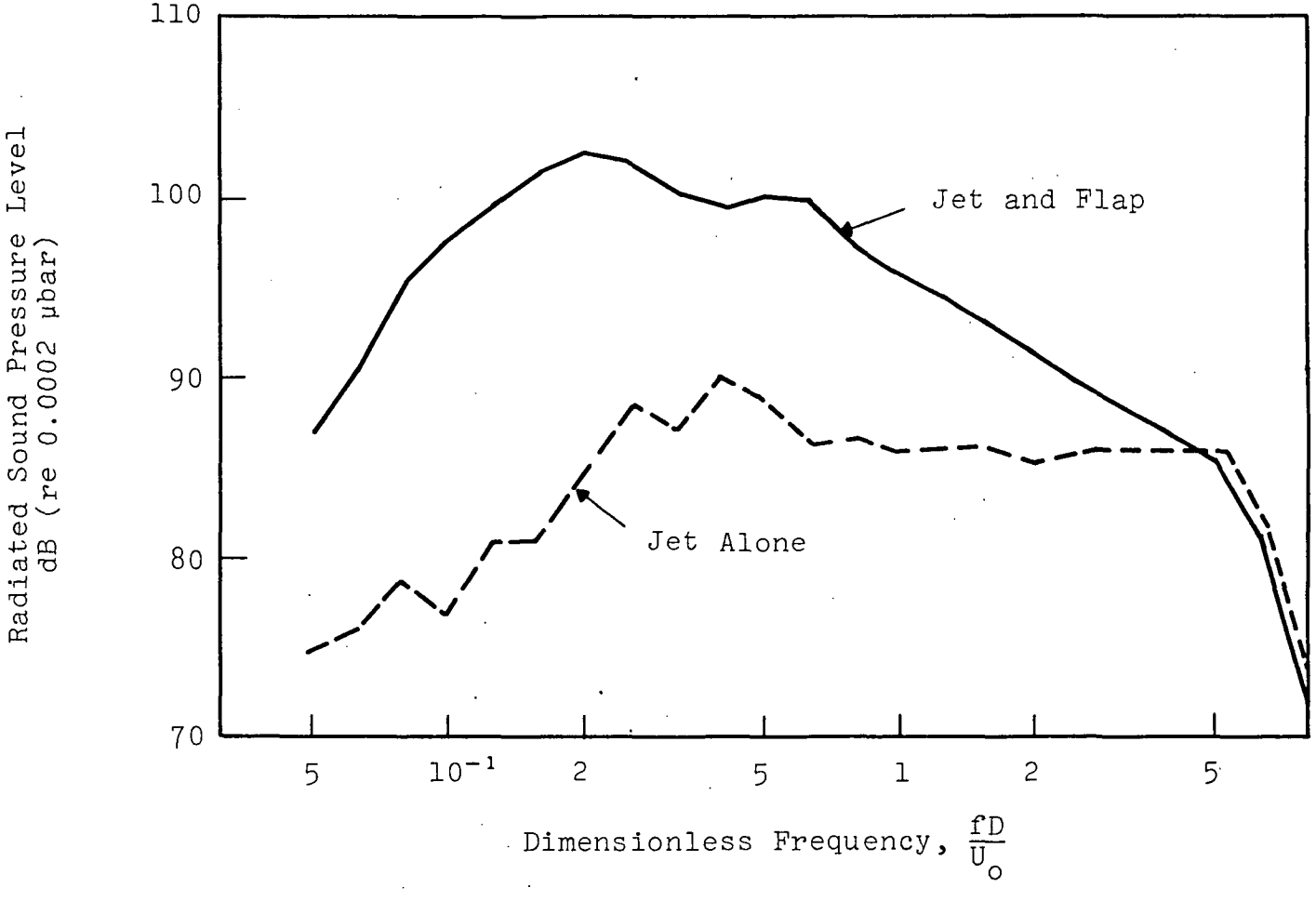

FIGURE 13. Sound Radiated by Jet and Flap and by Jet Alone (Configuration shown in Fig. 1, U_o = 550 ft/sec. Sound measured at an angle of 90° and distance of 1 ft from the jet axis.)

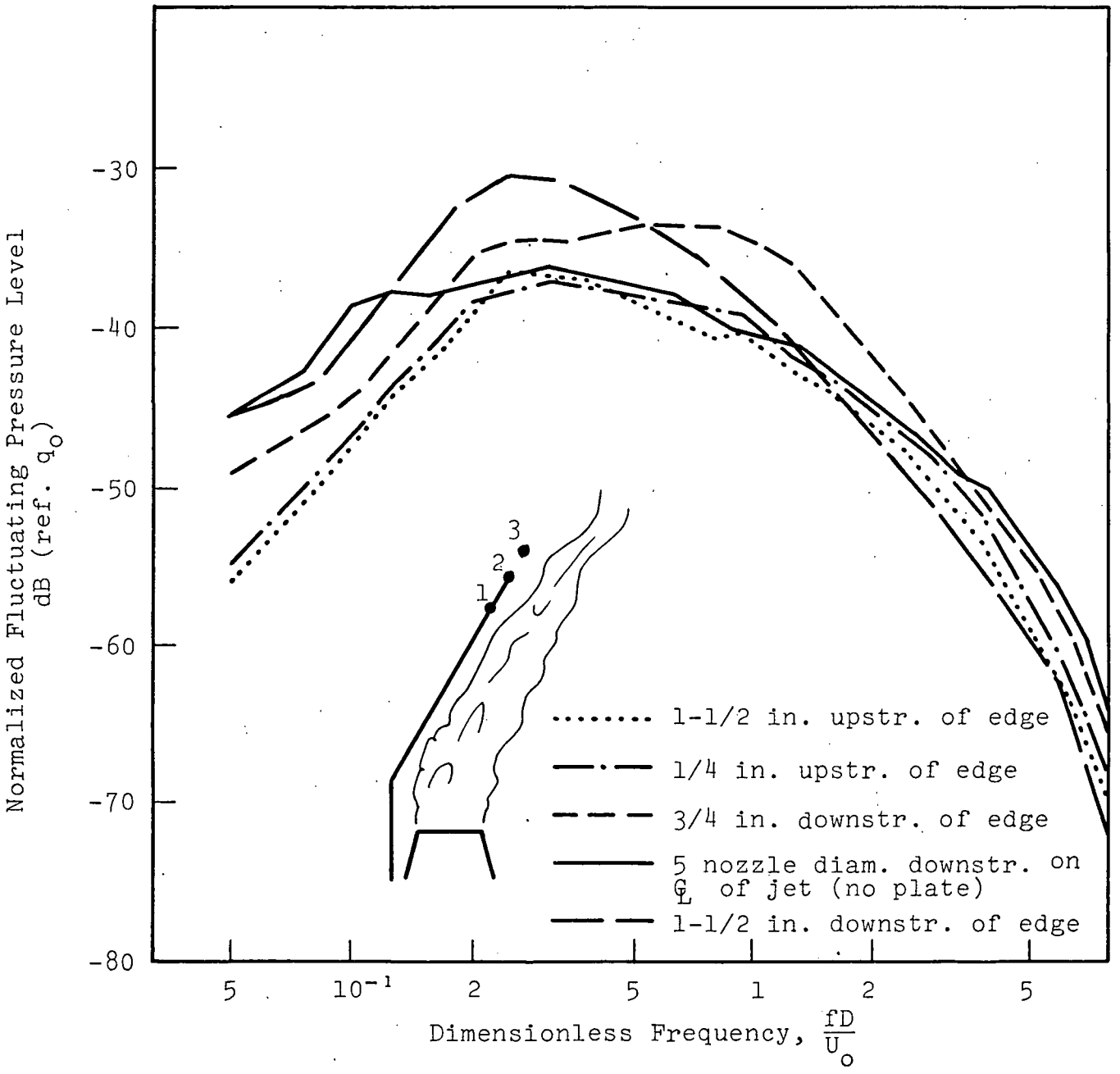

FIGURE 14. Surface and Jet Pressure Spectra (Configuration shown in Fig. 1, $V_o \approx 550$ ft/sec)

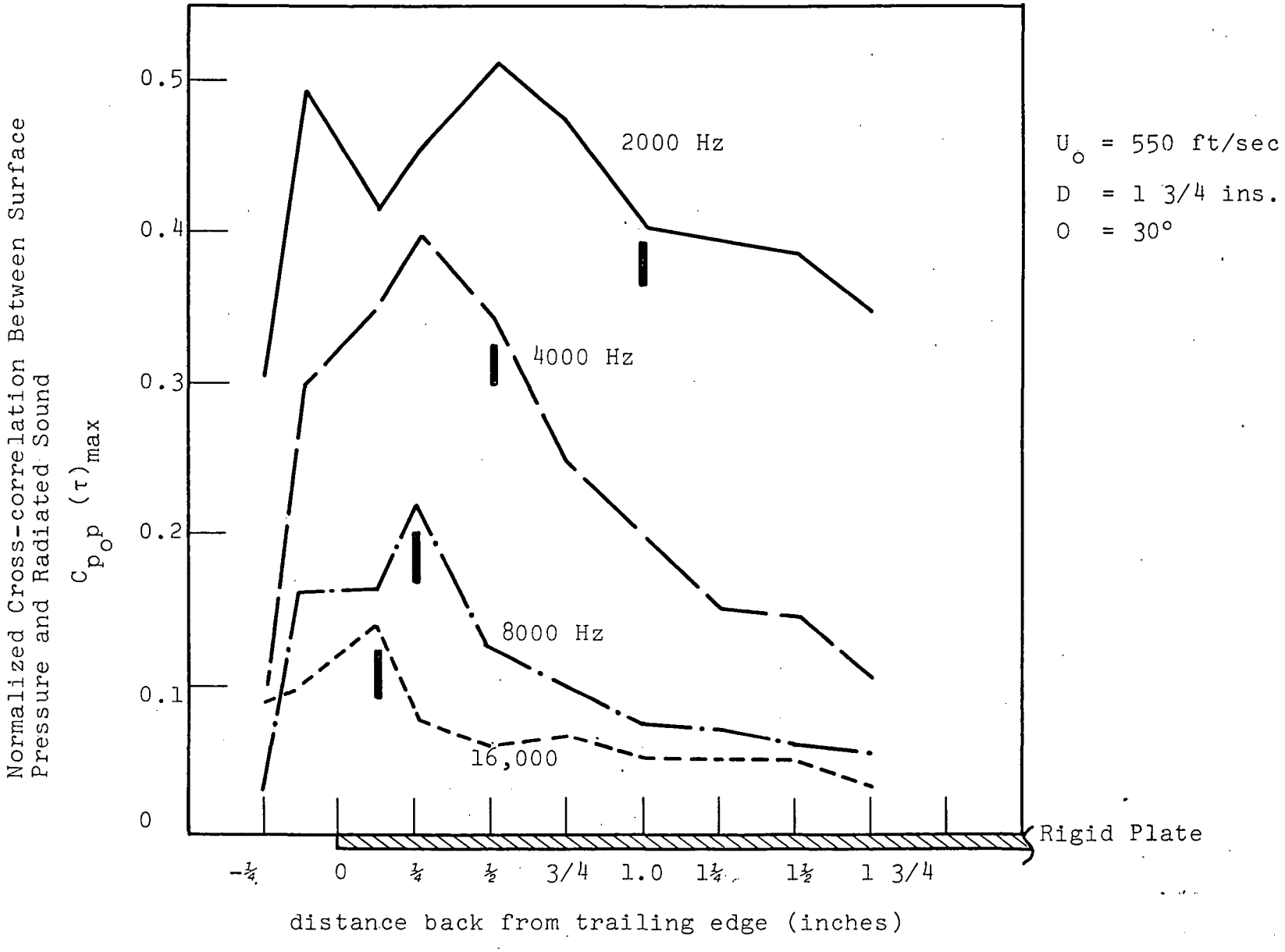

FIGURE 15. Cross-correlation of Radiated Sound and Surface Pressure Measured at Various Positions Back From Trailing Edge of Plate (Configuration as shown in Fig. 1, U_o = 550 ft/sec)

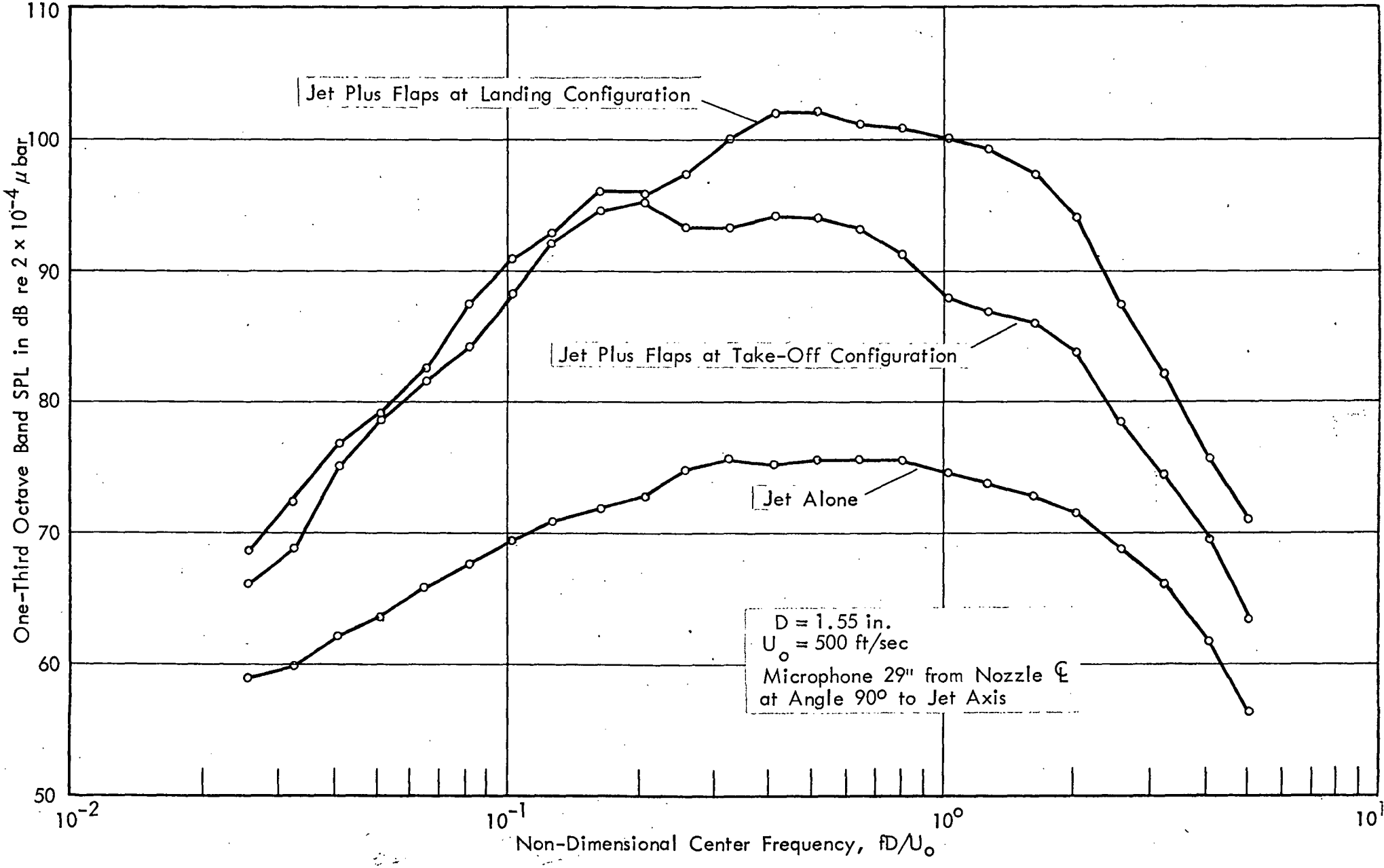

FIGURE 16. FAR FIELD SOUND RADIATED BY 1/15th SCALE 3-FLAP EBF SYSTEM

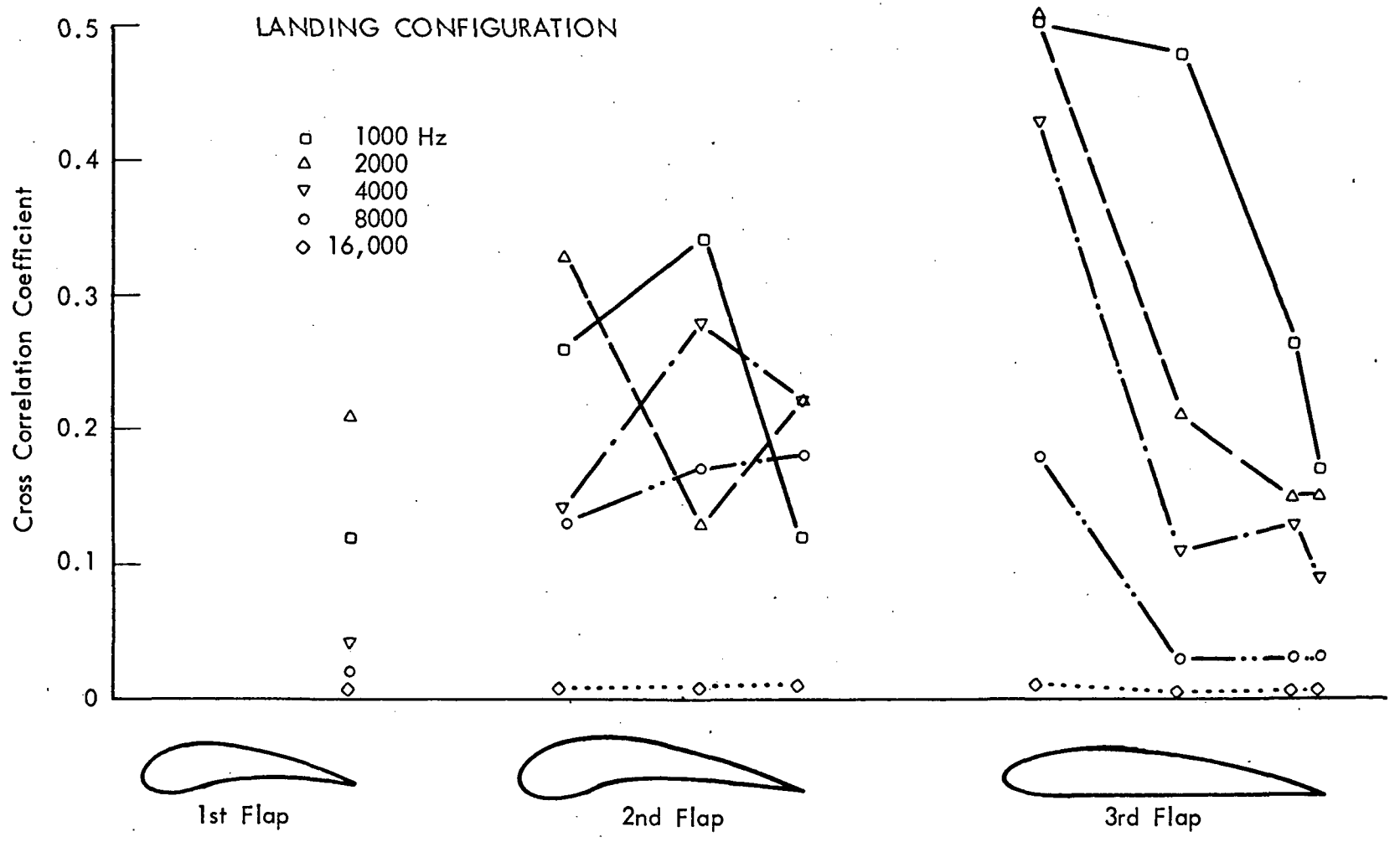

FIGURE 17. CROSS CORRELATION BETWEEN FAR FIELD PRESSURE AND LOCAL PRESSURE ON AIRFOIL (Landing Configuration)

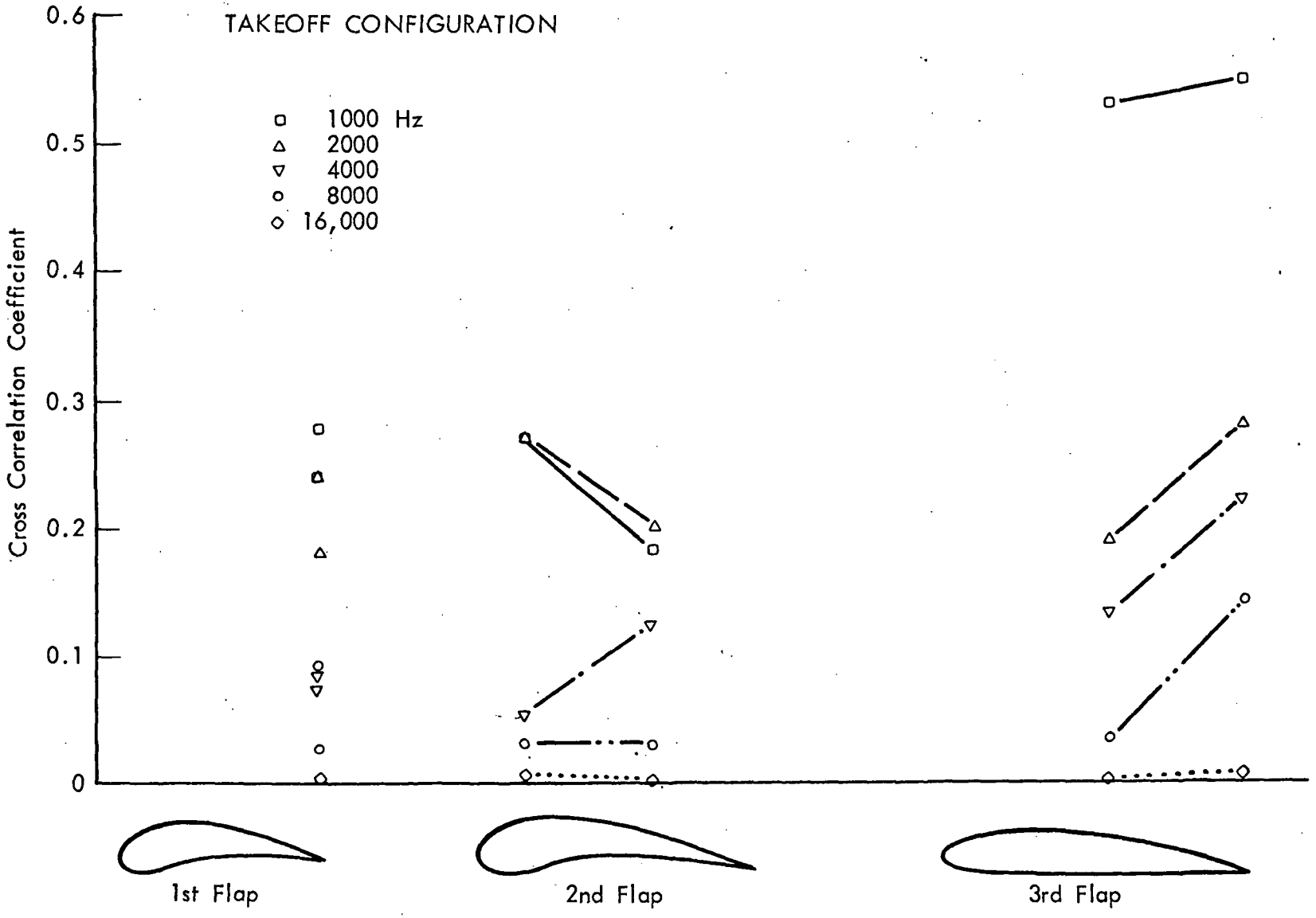

FIGURE 18. CROSS CORRELATION BETWEEN FAR FIELD PRESSURE AND LOCAL PRESSURE ON AIRFOIL (Take-Off Configuration)

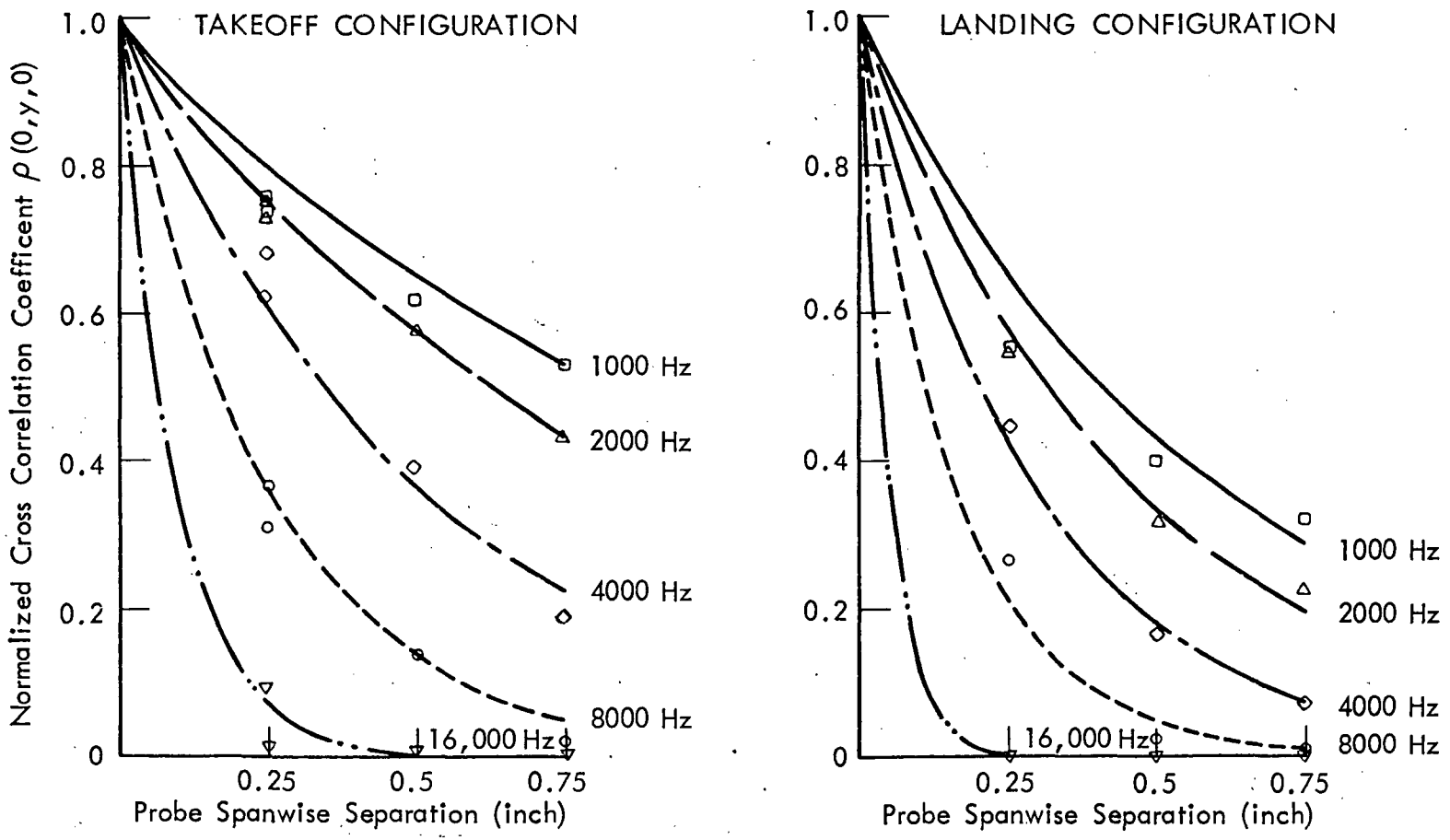

FIGURE 19. SPANWISE SPACE CORRELATION OF SURFACE PRESSURE AT TRAILING EDGE OF THIRD FLAP (Octave Bandwidth)

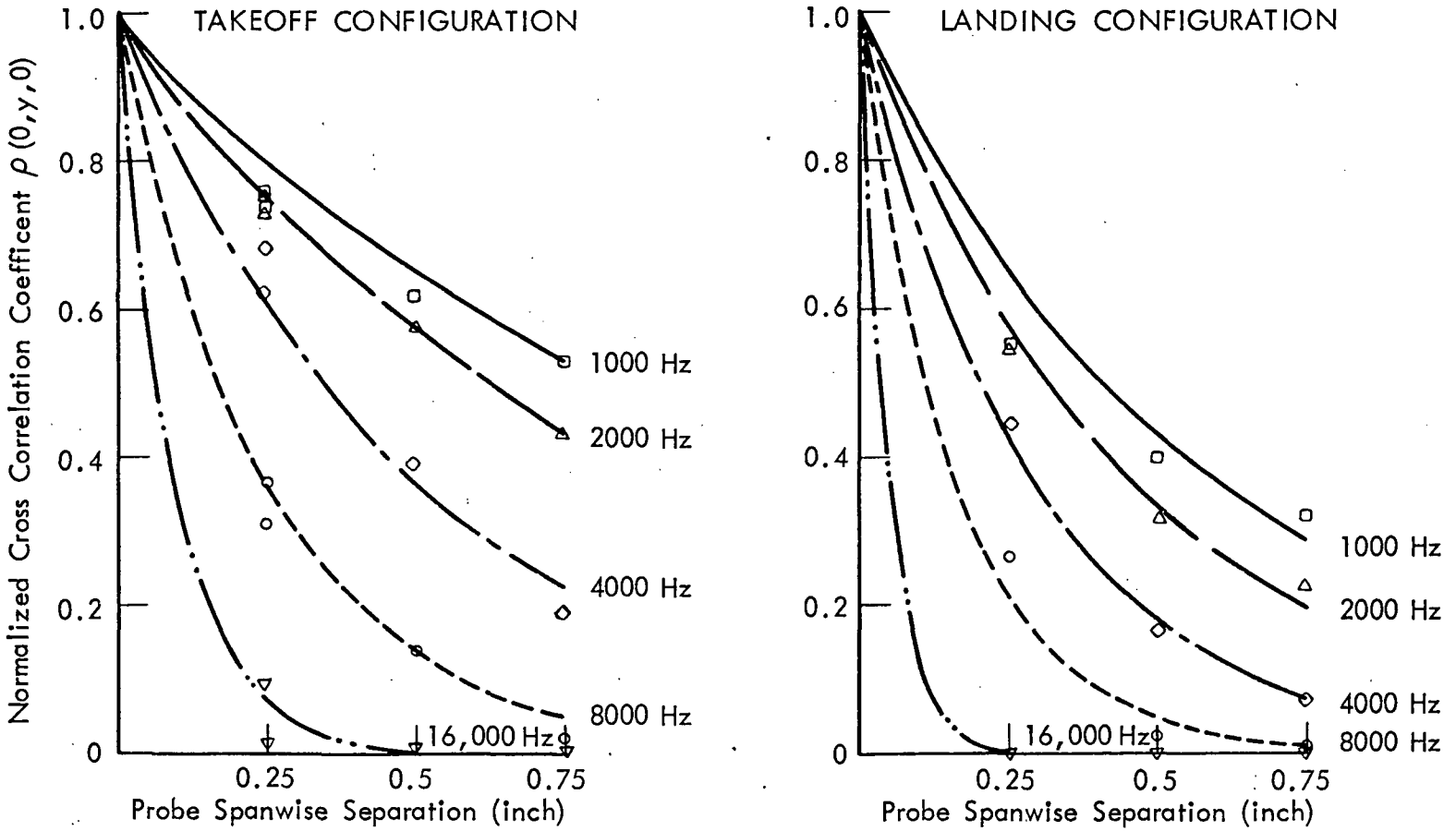

FIGURE 19. SPANWISE SPACE CORRELATION OF SURFACE PRESSURE AT TRAILING EDGE OF THIRD FLAP (Octave Bandwidth)

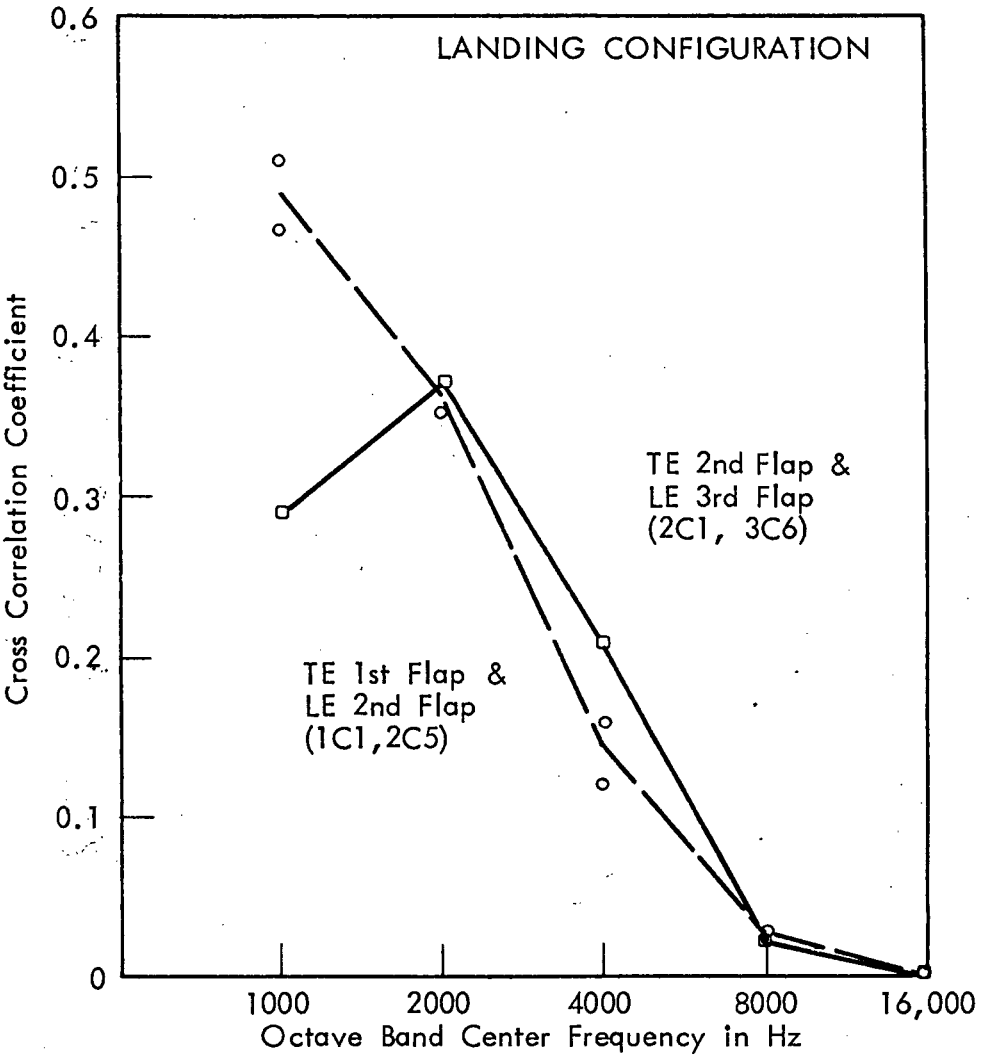

FIGURE 20. CORRELATION BETWEEN SURFACE PRESSURE ON TRAILING EDGE AND LEADING EDGE OF ADJACENT FLAPS

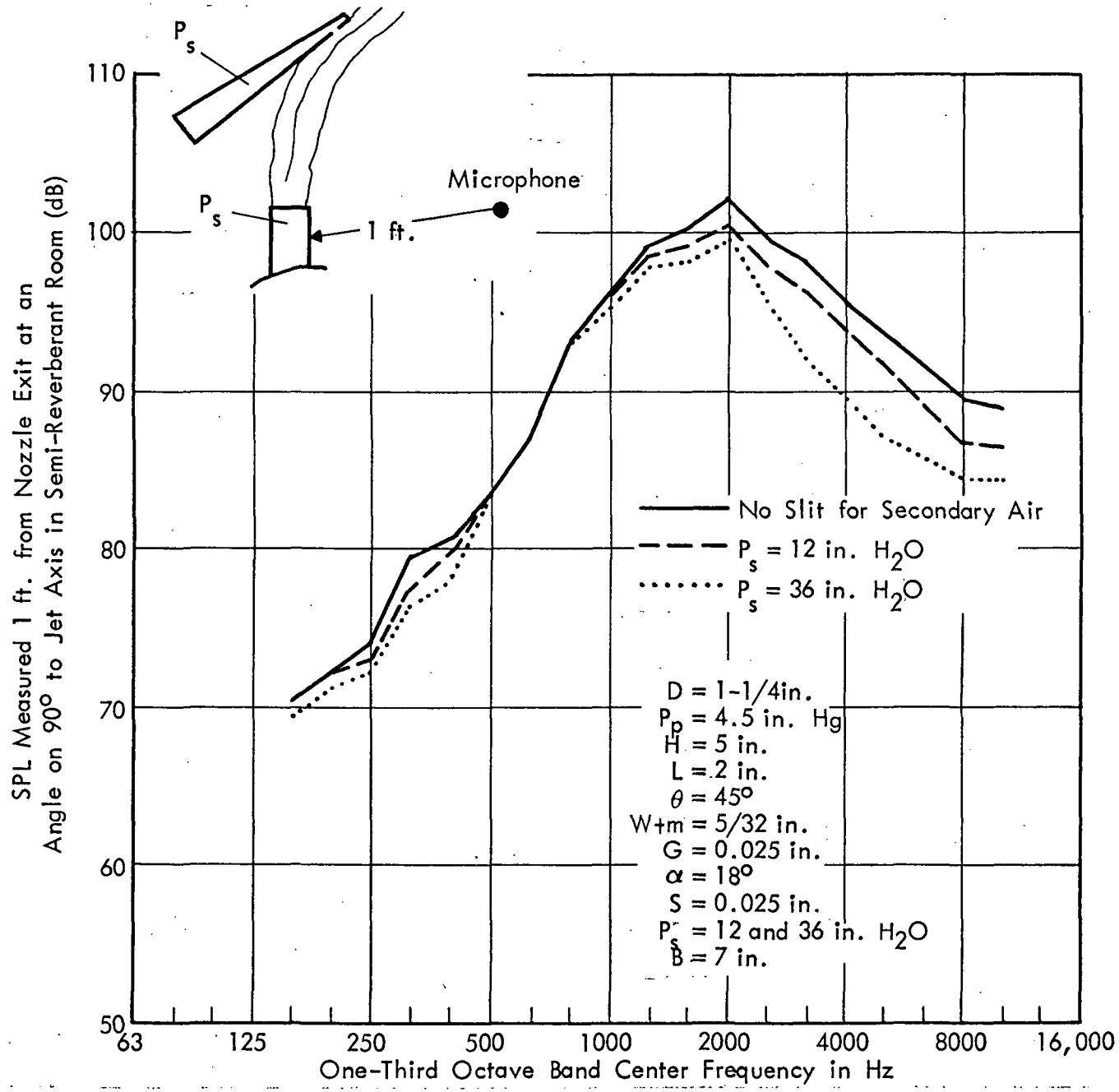

FIGURE 21. NOISE REDUCTION FOR 1.25" NOZZLE DIAMETER EDGE BLOWING CONFIGURATION (FIGS. 4,5)

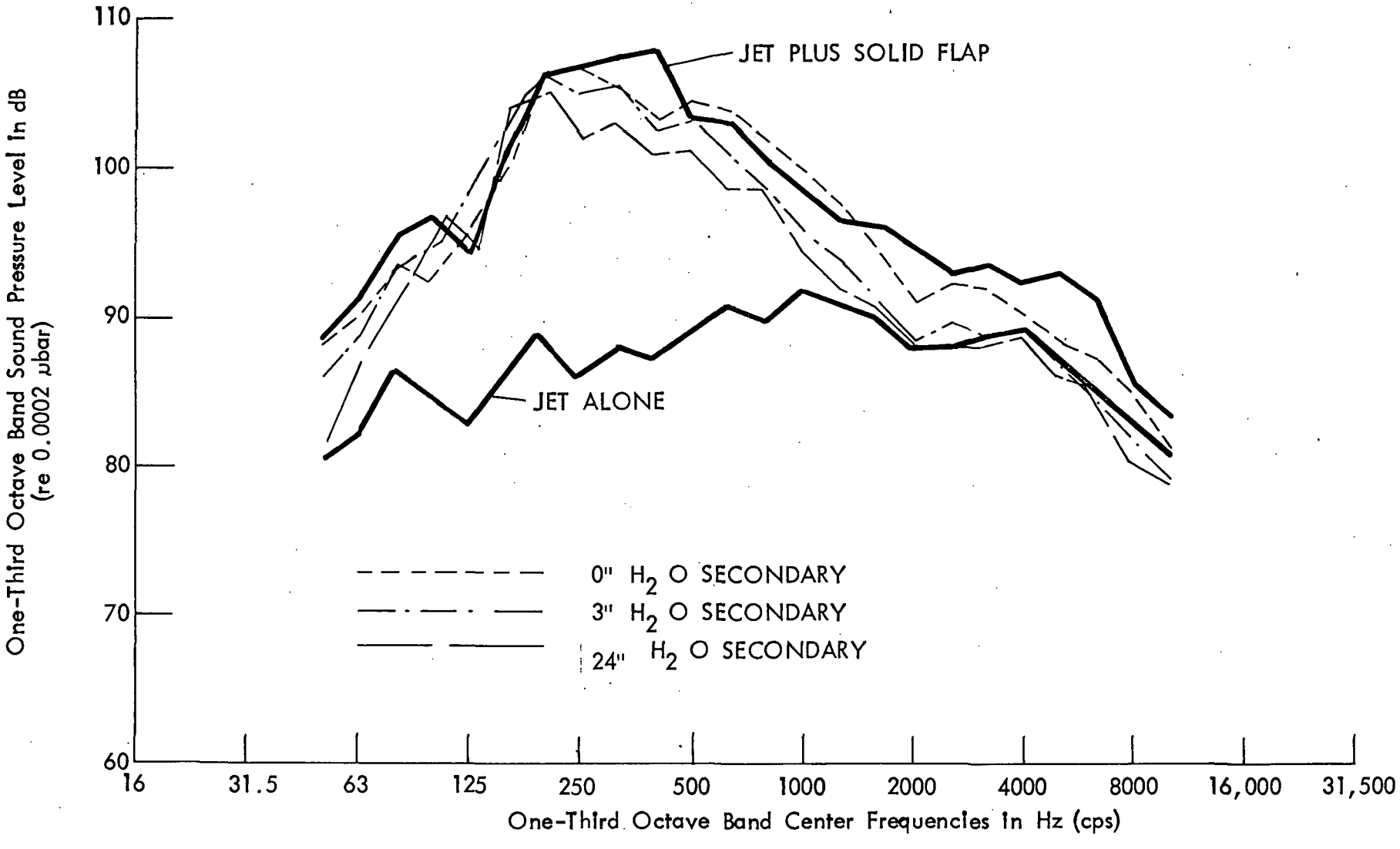

FIGURE 22. NOISE REDUCTION OBTAINED WITH TRAILING EDGE BLOWING ON 8" DIAMETER NOZZLE RIG AT MARQUARDT (CONFIGURATION 7B, 4.5 psig PRIMARY, GROUND MICROPHONE, FIGURE 11)

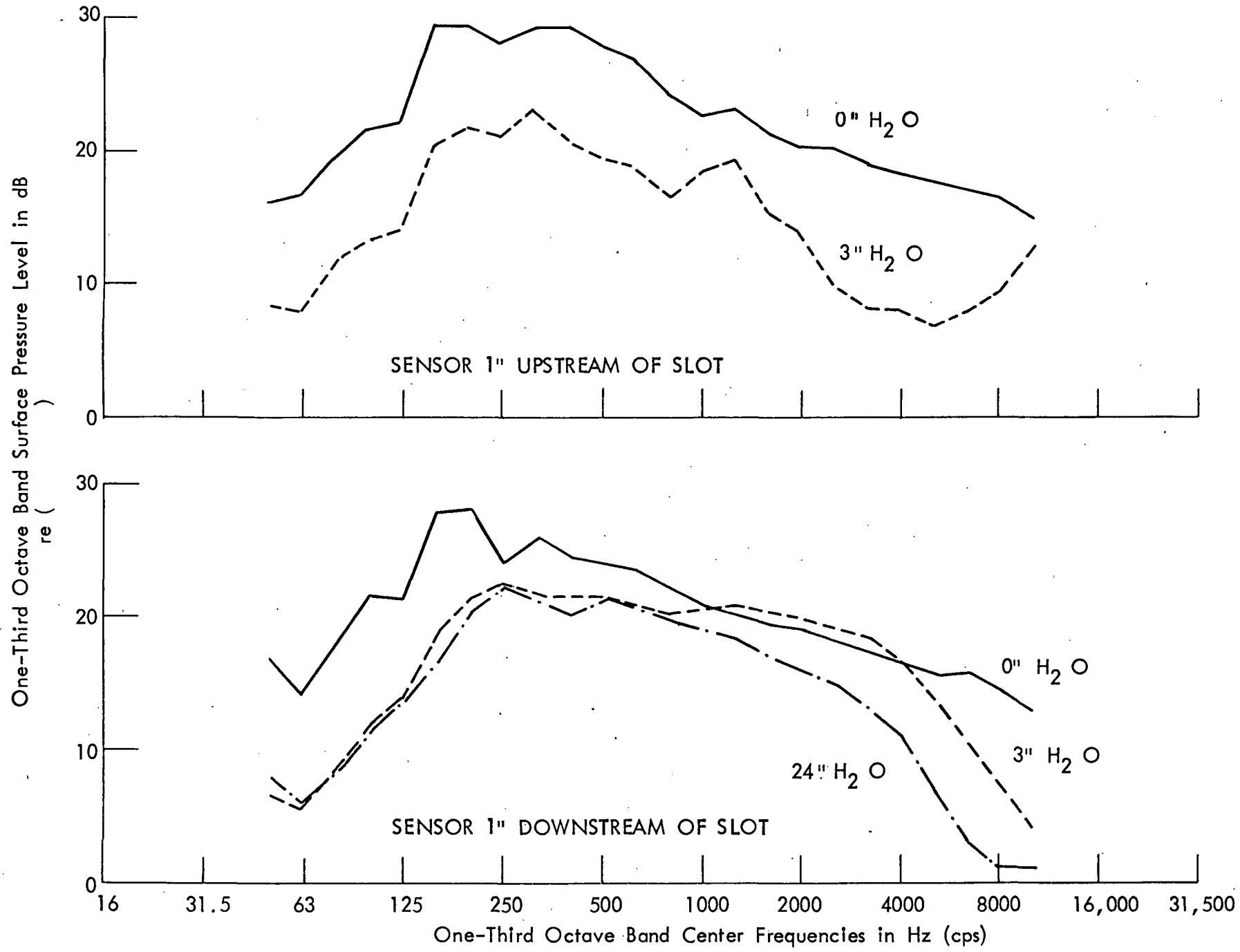

FIGURE 23. EFFECT OF SECONDARY AIR PRESSURE ON TRAILING EDGE SURFACE PRESSURES (PRIMARY AIR PRESSURE IS 4.5 PSIG)